Cranfield

College of Aeronautics Report 8329
November 1983

Bodies in Compressible Flow
– The Use of Axial Singularity Distributions

by P.A.T. Christopher and C.T. Shaw

College of Aeronautics
Cranfield Institute of Technology
Cranfield, Bedford, U.K.

Cranfield
College of Aeronautics Report 8329
November 1983

Bodies in Compressible Flow
– The Use of Axial Singularity Distributions

by P.A.T. Christopher and C.T. Shaw

College of Aeronautics
Cranfield Institute of Technology
Cranfield, Bedford, U.K.

ISBN 0 902937 95 2

£7.50

SUMMARY

A study has been made of techniques that could be used to extend axial singularity methods for incompressible flow, to deal with compressibility effects. In particular the accuracy of common linearisation methods has been investigated, together with methods for the iterative solution of the full potential equation using distributions of sources in the flow field. These field sources account for the non-linear terms in the equations, and a computer programme has been written to implement the method. For a range of body shapes, and subsonic Mach numbers, simple distributions of sources in the field lead to accurate results after only four iterations.

CONTENTS

1. INTRODUCTION.

Over the past three years, research has been carried out, at the College of Aeronautics, C.I.T., Cranfield (Refs. 1 to 4), into the use of axial singularity techniques for generating the flows around stream-lined bodies, and a range of useful methods have been developed. One major area of application of the work is in the calculation of the aerodynamic characteristics of aircraft fuselages, missiles, and aircraft stores. These techniques are inherently concerned with incompressible flow. However, the flow over an airframe and stores will probably be transonic for most of the flight, since the aircraft will probably be flying at high subsonic speeds close to the ground. It is obvious that some means of extending the previous methods to compressible flow is required.

Taking only the inviscid approximation for the flow (see Ref. 5, Chap, 7), the governing equations are non-linear, requiring a numerical/iterative solution throughout the flow field. In general, therefore, a flow solution demands not only that complicated geometries are dealt with, but also that the flow variables are determined everywhere in the field. At the present time, modern computing technology is still not capable of calculating flow problems in the general case, as Kutler emphasises in his recent review paper (Ref. 6). As a consequence of this, current computational software falls into two main categories:

a. Incompressible solution models which can solve complex geometries (e.g. panel methods, see Hess and Smith, Ref. 7), which are modified to solve a linearised form of the compressible flow equations in scaled a flow domain, i.e. using similarity laws. These methods are widely used, even though they are only strictly valid for small velocity perturbations and purely subsonic flow.

b. Full field method solutions for a limited range of specific cases such as aerofoils, wings, nacelles and bodies as described by Kutler in Ref. 6, which solve either the Euler or full potential equations, and can thereby deal with transonic flows and weak shocks.

As our own work has been concerned with the generation of incompressible flows by using axial distributions of singularities, we would like the capability of dealing with, at least, high subsonic Mach numbers, whilst still utilising the basic incompressible technique. This report presents the results of our investigations into posssible ways of extending incompressible flow methods to deal with compressibility effects. In particular three areas are investigated.

a. The accuracy of linearising the equations is investigated, together with the possibility of extensions to the linearisation process.

b. The method of a power series expansion in Mach number for spherical shapes is developed, and the question of extending it to more general shapes considered.

c. Solution of the full potential equation by re-writing it in a pseudo-Poisson form, and the placing singularities in the field to allow for compressibility.

By rewriting the pressure term of the momentum equation in the form

$$\frac{\partial p}{\partial x_i} = \left(\frac{\partial p}{\partial \rho}\right)_s \frac{\partial \rho}{\partial x_i} = a^2 \frac{\partial \rho}{\partial x_i}$$

and then transforming the momentum equation into a scalar equation by multiplying it by u_i , gives

$$u_i u_j \frac{\partial u_i}{\partial x_j} = - \frac{u_i}{\rho} \frac{\partial p}{\partial x_i} = - \frac{a^2}{\rho} u_i \frac{\partial \rho}{\partial u_i}$$

Combining this with the steady continuity equation 2.1.1 gives

$$u_i u_j \frac{\partial u_i}{\partial x_j} = a^2 \frac{\partial u_k}{\partial x_k} \qquad 2.1.8$$

Written out in terms of u, v, w, x, y, z , 2.1.8 becomes

$$\begin{aligned} &(u^2 - a^2)\frac{\partial u}{\partial x} + (v^2 - a^2)\frac{\partial v}{\partial y} + (w^2 - a^2)\frac{\partial w}{\partial z} \\ &+ uv\left(\frac{\partial u}{\partial y} + \frac{\partial v}{\partial x}\right) + vw\left(\frac{\partial v}{\partial z} + \frac{\partial w}{\partial y}\right) \\ &+ wu\left(\frac{\partial w}{\partial x} + \frac{\partial u}{\partial z}\right) = 0 \end{aligned} \qquad 2.1.9$$

Replacing the velocity components of 2.1.8 with the appropriate derivatives of the potential, the equation becomes

$$\frac{1}{a^2} \frac{\partial \phi}{\partial x_i} \frac{\partial \phi}{\partial x_j} \frac{\partial^2 \phi}{\partial x_i \partial x_j} = \frac{\partial^2 \phi}{\partial x_j \partial x_j} \qquad 2.1.10$$

We now have reduced the high speed flow equations to a single differential equation for the potential, ϕ ; the so-called full potential equation. Unfortunately this equation is non-linear, and so there is no general theory available which provides an exact solution. To overcome this, three alternative possibilities exist:

a. to obtain a numerical solution,

b. to transform the variables to make the equations linear, but still exact,

and c. to find linear equations which are an approximation to the exact non-linear ones.

Using modern computing techniques, numercial solutions are possible, if some-what expensive in computer run time and memory storage, and so linearised equations are still used in many situations to give economical results. With transonic flow, however, the equations are inherently non-linear, making the only approach a numerical one.

2.2 Linearisation of the Equations for Subsonic Flow - The Gothert Similarity Law.

Equation 2.1.9 can be linearised by using classical small perturbation methods, whereby the velocities are redefined as

$$\begin{aligned} u &= U_\infty + u' \\ v &= v' \\ w &= w' \end{aligned} \qquad 2.2.1$$

such that u'/U_∞, v'/U_∞ and w'/U_∞ are all very small. Using 2.1.7 in the form

$$\frac{u^2 + v^2 + w^2}{2} + \frac{a^2}{\gamma - 1} = \frac{U_\infty^2}{2} + \frac{a_\infty^2}{\gamma - 1} \qquad 2.2.2$$

and then substituting 2.2.2 and 2.2.1 into 2.1.7 we obtain

$$\left\{(U_\infty+u')^2 + \left(\frac{\gamma-1}{2}\right)\left((U_\infty+u')^2+v'^2+w'^2\right) - U_\infty^2\left(\frac{\gamma-1}{2}\right) - a_\infty^2\right\}\frac{\partial u'}{\partial x}$$
$$+\left\{ v'^2 + \left(\frac{\gamma-1}{2}\right)\left((U_\infty+u')^2+v'^2+w'^2\right) - U_\infty^2\left(\frac{\gamma-1}{2}\right) - a_\infty^2\right\}\frac{\partial v'}{\partial y}$$
$$+\left\{ w'^2 + \left(\frac{\gamma-1}{2}\right)\left((U_\infty+u')^2+v'^2+w'^2\right) - U_\infty^2\left(\frac{\gamma-1}{2}\right) - a_\infty^2\right\}\frac{\partial w'}{\partial z} \qquad 2.2.3$$
$$+ (U_\infty+u')v'\left(\frac{\partial u'}{\partial y} + \frac{\partial v'}{\partial x}\right) + v'w'\left(\frac{\partial v'}{\partial z} + \frac{\partial w'}{\partial y}\right) + w'(U_\infty+u')\left(\frac{\partial w'}{\partial x} + \frac{\partial u'}{\partial z}\right) = 0$$

Removing those terms containing products or squares of the small perturbation velocities u', v', w', on the grounds that they are negligible compared to the remaining terms, leads to the much simplified form

$$\left(U_\infty^2 + (\gamma+1)U_\infty u' - a_\infty^2\right)\frac{\partial u'}{\partial x} + \left((\gamma-1)U_\infty u' - a_\infty^2\right)\frac{\partial v'}{\partial y}$$
$$+ \left((\gamma-1)U_\infty u' - a_\infty^2\right)\frac{\partial w'}{\partial z} + U_\infty v'\left(\frac{\partial u'}{\partial y} + \frac{\partial v'}{\partial x}\right) \qquad 2.2.4$$
$$+ U_\infty w'\left(\frac{\partial w'}{\partial x} + \frac{\partial u'}{\partial z}\right) = 0$$

If it is further argued that terms containing $U_\infty u'$, $U_\infty v'$ and $U_\infty w'$ are also negligible, we obtain

$$\left(U_\infty^2 - a_\infty^2\right)\frac{\partial u'}{\partial x} + \left(-a_\infty^2\right)\frac{\partial v'}{\partial y} + \left(-a_\infty^2\right)\frac{\partial w'}{\partial z} = 0$$

or
$$\left(1 - M_\infty^2\right)\frac{\partial u'}{\partial x} + \frac{\partial v'}{\partial y} + \frac{\partial w'}{\partial z} = 0 \qquad 2.2.5$$

which is the final linearised form, valid for Mach numbers less than unity.

This equation can be solved by suitable scaling of the velocity potential, ϕ', and the space coordinates, as follows

$$\begin{aligned} \phi_i' &= m^2 \phi_c' \\ y_i &= m y_c \\ z_i &= m z_c \end{aligned} \qquad 2.2.6$$

where the scale factor $m=(1-M_\infty^2)^{\frac{1}{2}}$, the subscript c denotes a compressible flow quantity and subscript i refers to the scaled variables. Substitution of 2.2.6 into 2.2.5 shows that the scaled equation is, in fact, Laplace's equation, and so a solution of 2.2.5 can be found by calculating the incompressible flow over a scaled shape given by 2.2.6. This process is referred to as the Gothert transformation. The incompressible velocities are then transformed back to the compressible flow values by using the relationships

$$u_c' = \frac{\partial \phi_c'}{\partial x_c} = \frac{\partial(\phi_i'/m^2)}{\partial x_i} = \frac{1}{m^2} u_i'$$

$$v_c', w_c' = \frac{\partial \phi_c'}{\partial y_c, z_c} = \frac{\partial(\phi_i/m^2)}{\partial(y_i, z_i/m)} = \frac{1}{m} v_i', w_i' \qquad 2.2.7$$

Finally a relationship is sought for the pressure coefficient, defined as

$$C_p = \frac{p - p_\infty}{\frac{1}{2}\rho_\infty U_\infty^2} = \frac{2}{\gamma M_\infty^2}\left(\frac{p}{p_\infty} - 1\right) \qquad 2.2.8$$

For an isentropic gas, equations 2.1.3 and 2.1.7 combine to give

$$p_0/p = \left[1 + \left(\frac{\gamma-1}{2}\right)M^2\right]^{\gamma/\gamma-1} \qquad 2.2.9$$

This can now be substituted into 2.2.8, and using 2.1.7 to remove the sound-speed term, a^2, we obtain

$$C_p = \frac{2}{\gamma M_\infty^2}\left\{\left(1 + \left(\frac{\gamma-1}{2}\right)M_\infty^2\left(1 - \frac{|\bar{v}|}{U_\infty^2}\right)\right)^{\gamma/\gamma-1} - 1\right\} \qquad 2.2.10$$

A linearised form of 2.2.10 can be derived by substituting the small perturbation quantities of 2.2.1 into 2.2.10, and retaining only the second, or lower, order terms. Thus

$$C_p \approx -\frac{2u'}{U_\infty} - (1 - M_\infty^2)\frac{u'^2}{U_\infty^2} - \frac{(v'^2 + w'^2)}{U_\infty^2}$$

which can be approximated, ignoring the second term, for elongated bodies, by

$$C_p \approx -\frac{2u'}{U_\infty} - \frac{(v'^2 + w'^2)}{U_\infty^2} \qquad 2.2.11$$

Therefore, having calculated the flow over the scaled body, the pressure coefficient on that body will be given by

$$C_{pi} = -\frac{2u_i'}{U_\infty} - \frac{(v_i'^2 + w_i'^2)}{U_\infty^2}$$

and hence, using 2.2.7,

$$C_{pc} = -\frac{2u_i'}{U_\infty} - \frac{(v_i'^2 + w_i'^2)}{U_\infty^2} = -\frac{2}{U_\infty}\left(\frac{u_i'}{m^2}\right) - \left(\frac{v_i'^2}{m^2} + \frac{w_i'^2}{m^2}\right)\frac{1}{U_\infty^2}$$

or

$$C_{pc} = \frac{1}{m^2} C_{pi} \qquad 2.2.12$$

This last result enables incompressible solutions for flows around scaled bodies to be generated, and the resulting pressure coefficients converted back to obtain those on an unscaled body in compressible flow.

2.3 A Comparison of the Full Potential Equation Results with the Linearised Results.

An investigation has been carried out into the accuracy of the linearisation process, by comparing the subsonic axial flows over a range of shapes using both the linearised and full potential equations. In the first method a computer programme for the axi-symmetric

incompressible flow over bodies of revolution, written by Albone (Ref. 8), and based on Landweber's method (Ref. 9), has been applied to the scaled body, as in 2.2.6, and then a scaled pressure distribution obtained from 2.2.12. This, then simulates the linearised subsonic flow over the body at a given Mach number. Results from this programme have then been compared with those from the Aircraft Research Association (Bedford, U.K.) Solid Body Programme, which is a finite difference solution for the full potential equation in axi-symmetric flow. See Baker et al (Ref. 10) for details.

To represent a typical range of shapes, the comparisons are shown in Figs. 1 to 5 for a parabola of revolution, fineness ratio 10, at a Mach number of 0.8; an ellipsiod of fineness ratio 5, at Mach numbers 0.4, 0.6 and 0.8; and a sphere at a Mach number of 0.4. Agreement between the two methods is very good for the paraboloid, Fig. 1, except at the nose where the finite difference solution has a non-physical kink in the pressure distribution. This kink is due to the differencing scheme on the sharp nose giving the body slope as zero at the nose, and not the nose angle. On the ellipsiod, Figs. 2 to 4, the agreement is quite good at the lower Mach number, but becomes worse as the Mach number is increased. In particular, at two positions, the differences are noticeable; at the nose, where the stagnation pressure is not well predicted by the linearised method, and just after the rapid flow acceleration, where the linearised equations give a lower pressure coefficient than the full potential value. Clearly, at the nose the perturbation from the free stream velocity is the same magnitude as that velocity itself, and so the assumptions of linear theory break down, giving the larger error. The sphere, Fig. 5, shows similar trends to the ellipse, but whereas the linearised equations give a good prediction of the minimum pressure coefficient on the

ellipse, on the sphere they are again in error.

From these comparisons, the inadequacy of this form of linearisation is evident for bluff body shapes at high subsonic Mach numbers, and so to continue the investigation, an attempt at understanding the problem must be made by a closer examination of the equations.

2.4. Local Linearisation of the Equations

Although the Gothert scaling leads to errors in the actual values of the pressure distribution over bodies at certain flow conditions, the overall shape of the distribution is correct, and so, perhaps, the basic accuracy might be improved by reformulating the linearisation. As the form is correct, let us assume that the terms with derivatives $\partial u_i/\partial x_j (i \neq j)$ in 2.2.3 may be discarded, and that therefore the flow equation is given by

$$F\frac{\partial u'}{\partial x} + \frac{\partial v'}{\partial y} + \frac{\partial w'}{\partial z} = 0 \qquad 2.4.1$$

which is similar to 2.2.5, but with the scaling factor F replacing $(1 - M_\infty^2)$.

Taking 2.2.4 as the initial linearised form, by ignoring the terms above, the form of F is found to be

$$F = (U_\infty^2 + (\gamma+1)U_\infty u' - a_\infty^2)((\gamma-1)U_\infty u' - a_\infty^2)^{-1} \qquad 2.4.2$$

Expanding the second bracket in terms of $(\gamma-1)U_\infty u'/a_\infty^2$ and then ignoring the terms with products of u', we obtain

$$F = 1 - M_\infty^2\left(1 + \frac{2u'}{U_\infty} - (1-\gamma)M_\infty^2\frac{u'}{U_\infty}\right) \qquad 2.4.3$$

which further reduces, for small Mach numbers, to

$$F = 1 - M_\infty^2(1 + 2u'/U_\infty) \qquad 2.4.4$$

or

$$F = 1 - M_\infty^2\left(\frac{(U_\infty + u')^2}{U_\infty^2}\right)$$

This expansion is the same, using 2.2.11 for the pressure coefficient, as the 2-dimensional result of Weber, reported by Kuchemann (Ref. 19).

Previously, in Section 2.2, the scaling laws for the body radius, 2.2.6, and the velocity perturbations, 2.2.7, were stated in terms of the factor m, where

$$m = (1 - M_\infty^2)^{1/2}$$

Now from 2.4.4, m may be written as

$$m = \sqrt{F} = (1 - M_\infty^2 u^2/u_\infty^2)^{1/2} \qquad 2.4.5$$

Solution of the problem has been attempted in an iterative sense by scaling the original body shape using 2.4.5, with the incompressible velocity distribution over the body used for u/u_∞, and then iterating with more refined values of u/u_∞. Stagnation pressure coefficients are predicted exactly on blunt shapes, because the factor m goes to unity as the flow is brought to rest at the stagnation point, and so neither the body or the velocity perturbations are scaled at that point, giving the physically correct values. Unfortunately, as u/u_∞ increases near the point of maximum thickness of the bodies, so m reduces, and therefore the body radius is reduced abnormally. In some cases the body form is changed completely, as may be inferred from the pressure distribution over the new shape not being similar to the correct distribution, as in Fig. 6.

Despite these deficiencies, the form of 2.4.5 provides a qualitative insight into the validity of the Gothert scaling laws, by comparison of the body forms shown in Fig. 6 for both the Gothert scaling and the scaling using 2.4.5. At the front of the body, the

Gothert scaling produces far too high a pressure coefficient, as the velocity perturbations are scaled by dividing by m^2 or m which increases their magnitude, whereas, from 2.4.5, they should not be scaled at all, if u/u_∞ is zero. Away from the nose, a complex interaction between the body scaling and subsequent velocity perturbation scaling takes place. Where the flow velocity is less than its free stream value the Gothert scaled body is too thin, but the velocities are made correspondingly higher, and where the flow velocity is greater than the free stream value, the Gothert body is too thick, and the velocities made correspondingly lower. In the latter case, the errors cancel each other out, as the thicker body would have greater velocities on it, but these are reduced by the scaling factor. Nearer the front, however, where the flow is accelerating, the interaction between the body shape and the velocity distribution is not corrected by the Gothert scaling, as the results of Section 2.3 show.

Linearisation of the equations therefore leads to a quick and easy solution procedure for simulating the effects of compressibility by modifying incompressible flow calculation methods. For fine bodies, or low subsonic Mach numbers the results are good, compared to the full potential results, but on bluffer shapes the accuracy is reduced. Attempts to modify the scaling in an iterative sense are hampered by altering the body shape too much, giving an incorrect form for the pressure distribution, although they do provide some insight into the workings of the scaling laws. All in all, a more refined and accurate method of calculating the compressible flow over bodies is required.

3. SOLUTION OF THE COMPRESSIBLE FLOW EQUATIONS BY PERTURBATION TECHNIQUES

3.1 The Rayleigh-Janzen Expansion for Subsonic Flow.

Van Dyke (Ref. 11) lists many approximations using perturbation techniques, and describes the method of Rayleigh-Janzen for a circular cylinder in slightly compressible flow. Here the surface velocity is described as a perturbation from the incompressible flow solution using a series in M_∞^2 . Kaplan (Ref. 12) describes a similar method for a sphere in axi-symmetric flow.

Development of the method involves re-writing the basic equation 2.1.9 in potential form. Noting that from 2.2.2 we have

$$a^2 = f(\phi_x, \phi_y, \phi_z) \qquad 3.1.1$$

and if a_∞ , u_∞ are known, we can now see that 2.1.9 becomes

$$\nabla^2\phi = f(\phi_x, \phi_y, \phi_z, \phi_{xx}, \phi_{yy}, \phi_{zz}, \phi_{xy}, \phi_{xz}, \phi_{yz}) \qquad 3.1.2$$

The solution is formed by assuming that the potential, ϕ , can be developed as a power series in M_∞^2, such that

$$\phi = \phi_0 + \phi_1 M_\infty^2 + \phi_2 M_\infty^4 + \cdots \qquad 3.1.3$$

Substituting for ϕ in 3.1.2, and then equating the Mach number terms on each side gives a set of equations for the terms ϕ_n, see Kaplan (Ref. 12). In fact, ϕ_0 is shown to be the solution for the incompressible flow, and each successive term is the solution of Poisson's equation, where the right hand side depends only on the previous members of the series:

$$\nabla^2 \phi_n = f(\phi_{n-1}, \phi_{n-2}, \cdots, \phi_0) \qquad 3.1.4$$

Thus the series of 3.1.3, hopefully convergent, can be developed by a process of iteration from the basic incompressible solution.

Although the development above is straightforward, application of the method to different body shapes is hampered in several ways as follows:

a. The equations for ϕ_n become increasingly complex as n increases, leading to large amounts of tedious calculation.

b. Not only must the expressions for ϕ_n in 3.1.4 be satisfied, but also the boundary conditions of flow tangency on the surface and an undisturbed free stream at infinity must be satisfied. In the general case, an analytic form for ϕ_n can not be found directly, but the values for a sphere or ellipse can be found.

c. The series is believed (Van Dyke Ref. 11) to be convergent only if the value of the local Mach number remains below unity everywhere in the field. Thereby, transonic calculations can not be achieved.

3.2 Results for the Sphere in Axi-Symmetric Flow

Kaplan's analysis (Ref. 12) for the sphere in axi-symmetric flow, as shown in Fig. 7, gives the distribution of velocity over the surface taking = 1.408 for air, as

$$|\bar{v}|/|\bar{v}_\infty| = 1.5 \sin\theta + \frac{1}{7040}(989\sin\theta - 1215\sin 3\theta) M_\infty^2 \qquad 3.2.1$$

$$+(0.11048\sin\theta - 0.17018\sin 3\theta + 0.07489\sin 5\theta) M_\infty^4 \ldots$$

Equation 2.2.10 can now be used to give the surface pressure distribution, and in Fig. 8 the results are plotted for two Mach numbers, 0.40 and 0.57, using powers of Mach number up to four, together with the results of the ARA finite difference programme at the same conditions. This figure shows that the first three terms of the expansion give a sufficiently accurate calculation, provided that the local Mach number is not too close to unity, as at a Mach number of 0.57 the solutions are not as close as at a Mach number of 0.4, due to the slower convergence where the flow speed is nearly at the local sound-speed. Having demonstrated the capability of the method, it is now worth exploring to see if the method can be extended to a greater range of body shapes.

3.3 Possibilities of Extending the Method.

As mentioned in Section 3.1, the form of each ϕ_n must not only satisfy 3.1.4, but it must also satisfy the boundary conditions, and to do this analytically involved finding a suitable Green's function (see Kellogg, Ref. 13) for each body shape. For the spherical or elliptic shapes this is possible, but in general it is not. However, it may be possible to overcome these problems by numerically finding the solution to a series of Poisson equations.

Two approaches could be made, either to solve the equation set 3.1.4 for each ϕ_n, or to solve the main equation 3.1.2. In either case, the right hand side can be equated to a distribution of sources in the flow whose strength is calculated from the previous iteration. Physically we can imagine an field of sources in the flow. These sources induce velocities at the body surface which violate the boundary conditions, and in themselves generate further sources in the field, making an iterative technique necessary.

Whilst our studies were in progress, the works of Slooff (Ref. 14) and Johnson et al (Ref. 15) were published, which used a basic incompressible panel method solution (see Hess and Smith, Ref. 7), with an iterative Poisson-type solution. Our own approach is similar to that of Slooff, and this we will now describe.

4. SOLUTION OF THE FULL POTENTIAL EQUATION FOR AXI-SYMMETRIC FLOW BY THE USE OF FIELD SOURCES

4.1 An Outline of the Method.

Within Section 2.1 we detailed the equations of compressible flow, leading to the full potential equation 2.1.10. To deal with axi-symmetric body shapes, it is useful to work in cylindrical coordinates (r , θ , x), in which system the full potential equation becomes (see Reyhner, Ref. 16)

$$\begin{aligned}&(a^2-\phi_x^2)\phi_{xx} + (a^2-\phi_r^2)\phi_{rr} + (a^2-\phi_\theta^2/r^2)\phi_{\theta\theta}/r^2 \\ &-2\phi_x\phi_r\phi_{xr} - 2\phi_r\phi_\theta\phi_{r\theta}/r^2 \\ &-2\phi_\theta\phi_x\phi_{\theta x}/r^2 + \left(a^2+\phi_\theta^2/r^2\right)\phi_r/r = 0\end{aligned} \qquad 4.1.1$$

and the energy equation 2.2.2 becomes

$$a^2 = a_\infty^2 - \left(\frac{\gamma-1}{2}\right)\left(\phi_x^2 + \phi_r^2 + \phi_\theta^2/r^2 - |\bar{V}_\infty|^2\right) \qquad 4.1.2$$

The present development has been restricted to axi-symmetric flow alone, and so all the derivatives with respect to θ are zero. Thus the equations reduce, with a rearrangement, to the following:

$$\phi_{rr} + \phi_{xx} + \phi_r/r = \frac{\phi_x^2\phi_{xx}}{a^2} + \frac{\phi_r^2\phi_{rr}}{a^2} + \frac{2\phi_x\phi_r\phi_{xr}}{a^2} \qquad 4.1.3$$

and

$$a^2 = a_\infty^2 - \left(\frac{\gamma-1}{2}\right)\left(\phi_x^2 + \phi_r^2 - |\bar{V}_\infty|^2\right) \qquad 4.1.4$$

Noting that the left hand side of 4.1.3 is the Laplacian operator, ∇^2, we see that the equation may be written as

$$\nabla^2 \phi = f(\phi_x, \phi_r, \phi_{xx}, \phi_{xr}, \phi_{rr}) = F_{DIV} \qquad 4.1.5$$

where

$$F_{DIV} = \frac{1}{a^2}\left(\phi_x^2 \phi_{xx} + \phi_r^2 \phi_{rr} + 2\phi_x \phi_r \phi_{xr}\right) \qquad 4.1.6$$

To complete the problem, boundary conditions have to be applied at the body surface, where the flow must be tangential to the surface, i.e. for an axi-symmetric body

$$\phi_r - \left(\frac{dr}{dx}\right)_{body} \phi_x = 0 \qquad 4.1.7$$

and at infinity, where the free stream must be undisturbed

$$\nabla . \phi \Big|_\infty = u_\infty \qquad 4.1.8$$

Equation 4.1.5 is basically Poisson's equation, where the right hand side represents a divergence in the field, or in other words, a distribution of sources throughout the field. To solve the problem, let us consider that the potential, ϕ, is made up of two components; ϕ_F, that due to the divergence, F_{DIV}, in the field, and ϕ_A, that due to the body, which will be described as a distribution of axial sources, $f(\xi)$. This necessarily limits the class of body which can be considered, as described in Ref. 1. See Fig. 9.

Therefore

$$\phi = \phi_A + \phi_F + \phi_{\text{Free stream}} \qquad 4.1.9$$

where

$$\phi_A = -\frac{1}{4\pi}\int_0^L \frac{f(\xi)}{\{(x-\xi)^2+r^2\}^{1/2}}\, d\xi \qquad 4.1.10$$

and

$$\phi_F = -\frac{1}{4\pi}\iiint_V \frac{F_{DIV}}{R}\, dV \qquad 4.1.11$$

As equation 4.1.5 is non-linear, an iterative solution procedure has to be adopted enabling refined estimates of ϕ to be calculated. Our previous work (Ref. 1) has developed an accurate solution procedure for axi-symmetric bodies in incompressible, axial flow using axial distributions of sources, and so this solution can be used as a starting solution, ϕ_{A_1}. From ϕ_{A_1} a first approximation to the field distribution, F_{DIV_1}, can be found using 4.1.6. The left hand sides of the equations 4.1.5 and 4.1.7 are linear and so a matrix solution can be found using the approximation to F_{DIV} as the right hand side of 4.1.5, for the values of the axial source distribution and the field source distribution, giving ϕ_{A_2} and ϕ_{F_2}. These two now define a new distribution of F_{DIV}, enabling the process to continue as before, until the value of the total potential, ϕ, satisfies both 4.1.5 in the field, and 4.1.7 on the surface.

4.2 Description of the Singularity Potentials and their Derivatives.

Numercal calculation of the values of ϕ_A and ϕ_F is dependent on an approximation being made for the source distributions, both on the axis and in the field. Our paper, Ref. 1, describes the use of

axial source distributions for axi-symmetric bodies in incompressible, axial flow, based on the description of the source strength function, by a series of segmented polynomials of the form

$$f_k(\xi) = \sum_{n=0}^{N_k} c_n \xi^n \qquad 4.2.1$$

where $f_k(\xi)$ is the distribution strength in segment k, and N_k is the degree of the polynomial in that segment. From 4.1.10 the values of the five derivatives of ϕ_A can be found to be:

$$\begin{aligned}
\phi_x &= \frac{1}{4\pi}\int_0^L \frac{f(\xi)(x-\xi)}{\{(x-\xi)^2+r^2\}^{3/2}}\,d\xi \\
\phi_r &= \frac{r}{4\pi}\int_0^L \frac{f(\xi)}{\{(x-\xi)^2+r^2\}^{3/2}}\,d\xi \\
\phi_{xx} &= \frac{1}{4\pi}\int_0^L f(\xi)\left\{\frac{1}{\{(x-\xi)^2+r^2\}^{3/2}} - \frac{3(x-\xi)^2}{\{(x-\xi)^2+r^2\}^{5/2}}\right\}d\xi \qquad 4.2.2 \\
\phi_{rr} &= \frac{1}{4\pi}\int_0^L f(\xi)\left\{\frac{1}{\{(x-\xi)^2+r^2\}^{3/2}} - \frac{3r^2}{\{(x-\xi)^2+r^2\}^{5/2}}\right\}d\xi \\
\phi_{xr} &= \frac{-3}{4\pi}\int_0^L \frac{f(\xi)(x-\xi)r}{\{(x-\xi)^2+r^2\}^{5/2}}\,d\xi
\end{aligned}$$

Combining 4.2.2 with 4.2.1, the form of the integrals is given by

$$I = \int_a^b \frac{\xi^n}{\{(x-\xi)^2 + r^2\}^{(2m+1)/2}}\,d\xi \qquad 4.2.3$$

This is a standard integral whose solution is given by Gradstein and Ryshik (Ref. 17) in the form of a recurrence relationship, and Ref. 1 gives details of the computation.

To describe the field source distribution, F_{DN}, use is made of the property of axi-symmetric flow that there is no variation with angle θ. Thus F_{DN} is constant at any given position (x_j, r_j), and the source distribution can be assumed to be a set of rings. From Fig. 10, the distance R between a general field point P and a field source point Q, is given by

$$R^2 = \left\{ (x_j - x_s)^2 + r_j^2 + r_s^2 + 2 r_j r_s \sin(K - \theta_s) \right\}$$

Taking θ_j as zero, for simplicity, then

$$R = \left\{ (x_j - x_s)^2 + r_j^2 + r_s^2 + 2 r_j r_s \sin(k) \right\}^{1/2} \qquad 4.2.4$$

In discretising the flow field, small elements of area are defined, and their centroids calculated. The integration 4.1.11 can then be carried out by assuming that a ring is placed through the centroid to give

$$\phi_F = -\frac{1}{4\pi} \sum_{VOL} \left(\int_0^{2\pi} \frac{F_{DN}(x,r)\, r_s}{R} \right) \delta A \qquad 4.2.5$$

As the ring position moves further from the body, the flow disturbances on the free stream flow reduce to zero, and so from 4.1.6 the value of F_{DN} goes to zero. This enables the source rings to be placed in a restricted volume of fluid, near the body, as an approximation to placing them throughout the whole field. Thereby, the magnitude of the computation can be reduced. For each ring the derivatives of ϕ

are given by

$$\phi_x = \frac{1}{4\pi}\int_0^{2\pi} \frac{F_{DIV}\, r_s (x_f - x_s)}{R^3}\, dk$$

$$\phi_r = \frac{1}{4\pi}\int_0^{2\pi} \frac{F_{DIV}\, r_s (r_f + r_s \sin k)}{R^3}\, dk$$

$$\phi_{xx} = \frac{1}{4\pi}\left\{ \int_0^{2\pi} \frac{F_{DIV}\, r_s}{R^3}\, dk - \int_0^{2\pi} \frac{3(x_f - x_s)^2 F_{DIV}\, r_s}{R^5}\, dk \right\} \qquad 4.2.6$$

$$\phi_{rr} = \frac{1}{4\pi}\left\{ \int_0^{2\pi} \frac{F_{DIV}\, r_s}{R^3}\, dk - \int_0^{2\pi} \frac{3F_{DIV}\, r_s (r_f + r_s \sin k)^2}{R^5}\, dk \right\}$$

$$\phi_{xr} = \frac{-3}{4\pi}\int_0^{2\pi} \frac{F_{DIV}\, r_s (x_f - x_s)(r_f + r_s \sin k)}{R^5}\, dk$$

where R is given by 4.2.4, and the total effect of each fluid element is found by multiplying each of 4.2.6 by the elemental area δA . See Appendix A for a discussion of the stability of these field distributions.

Calculation of the elliptic integrals 4.2.6 can be carried out in two ways, either numerically or by a standard solution routine available in the NAG library (Ref. 18). In terms of calculation time, no appreciable difference has been found between the two methods, and so a numerical solution is used.

4.3 Computational Details of the Field Source Method.

Section 4.1 described the basic technique for the use of a field distribution of sources in solving compressible flow problems, and this has been translated into a computational routine for compressible axi-symmetric flow, on the Cranfield VAX 11/782 computer using a main FORTRAN programme with eight major subroutines. This programme has

been written in a simple form to give an initial evaluation of the method.

4.3.1 Input Data

To describe the flow situation, the body shape is input as a series of (x,r) coordinates from which all other values can be interpolated, plus a pointer to indicate either a sharp or blunt nose. The calculation is carried out at a given Mach number for a pre-set number of iterations. Finally, the axial source distribution parameters of segment position and polynomial degree are input, together with the field source distribution parameters defined in Fig. 11.

4.3.2 The Discretisation of the Field.

Field sources are placed in a given region of fluid around the body in three areas; ahead of the nose, along the length of the body, and behind the tail of the body. Each area is then divided into a number of rectangular or triangular patches as in Fig. 11. Within each patch, the source ring is placed at the centroid, and so the centroid coordinates are calculated, together with the area of the patch.

4.3.3 An Incompressible Solution.

As a starting solution for the iteration process, the programme calculates the axial source distribution for the body in incompressible flow, i.e. with no field sources. Using previous experience (Ref. 1) with axial source distributions, suitable sets of segment locations and polynomial degrees are chosen, to give a good representation of the body shape. Any axial singularity method is strictly limited to bodies

with analytic surface streamlines, having a nose shape that is not too bluff, although, as we demonstrated in Ref. 1, many reasonable shapes outside these limits can be generated.

In the previous work, the source distribution was found by applying both the flow tangency boundary condition and the "zero stream function value" condition at a set of control points. Here, when the compressible flow is considered, a stream function can not be defined, and so we have applied only the flow tangency condition. This enables us to ensure that the flow model is capable of giving a good representation before proceeding into the compressible calculation routine. Fifty boundary control points are used, distributed either at equal spacing for sharp nosed bodies, or with a cosine variation for blunt nosed bodies. The coefficients of the source distribution, which must be fifty or less in number, are then found using the least squares solution procedure of the NAG library (Ref. 18), F04JAF.

As a check on the accuracy of the solution, the pressure distribution and boundary condition error on the body are calculated and then output, before the compressible calculation routine is entered.

4.3.4 The Compressible Calculation Procedure.

At the beginning of each iteration, approximations to the two singularity distributions, one in the field and the other on the axis, are known to the programme. Initially, the axial distribution will be the incompressible solution, and the field distribution will be zero everywhere. From these, the effect of each source ring in the field, in terms of the five derivatives of the potential, given by 4.2.6, can be summed together, and the influence of the axial distribution, 4.2.2, added to it, at a set of field points in the meridian plane. Then, using 4.1.4 and 4.1.6, the value of the new ring strength at each position is found. If the local Mach number is greater than unity, two possible flow solutions could occur, one of which would have expansion shocks. In the real flow, the fluid viscosity would prevent such solution occuring, and so a damping term is added here to stabilise the solution:

$$F_{DN} = (\phi_r^2 \phi_{rr} + \phi_x^2 \phi_{xx} + 2\phi_x \phi_r \phi_{xr})/a^2 - k_v \phi_{xxxx} \qquad 4.3.1$$

The left hand side of 4.1.3 is calculated at each point, and its value output, together with the new field source strength, so that a check can be made on the convergence of the process in the field.

On the first iteration only, the influence matrix is set up by writing the left hand side of the boundary condition equation 4.1.7 in terms of all the source coefficients at the same fifty surface points as those in the incompressible solution. To this, the matrix is completed by adding the left hand side of 4.1.5 at each field point, written in the same terms. The matrix is then stored on disc to facilitate its retrieval in the next iteration, as the solution

procedure destroys the matrix stored in the internal memory.

A solution vector for the influence matrix is assembled from 4.1.7 and 4.1.5 in terms of the free stream velocity and the latest field source distribution, and, where necessary, the influence matrix is re-assembled from the disc. Then the NAG routine F04JAF solves for the source coefficients, both in the field and on the axis, enabling the process to begin again if required.

When the preset number of iterations are complete the pressure distribution is calculated along the body surface, and the results output. This terminates the calculation, and the programme is stopped.

4.4 *Some Results Using the Field Source Method.*

4.4.1 Parabolae of Revolution.

In describing the flow of a compressible fluid, the full potential equation 4.1.3 should define, for a given body shape, the value of potential, ϕ , everywhere. As with all numerical methods, the field source method approximates the function ϕ using a polynomial description for sources on the axis, and a set of source rings outside the body. Our initial work (Ref. 1) showed that the axial source description is highly accurate, and so we must now evaluate the accuracy of the field source rings as their distribution in the flow field is varied. Thereby an accurate solution can be obtained for the minimum compuational effort.

Using the parabola of revolution, with a fineness ratio of 10, at a Mach number of 0.8, an initial study of the method has been carried out. Here the flow is subsonic throughout the field, and the body should cause only small perturbations from the free stream flow, giving a relatively easy flow to model. Even so, with only 160 field rings, the time for solution is large, being of the order of one hour for four iterations on the VAX 11/782 computer. Hence, to reduce cost the minimum number of runs has been performed, and so the convergence study is not as full as would have been liked. Despite these drawbacks, the important trends have been found from the few sets of data obtained. One main feature of the method is the rate of convergence of the solution, both in terms of matching the left and right hand sides of 4.1.3 and the surface pressure coefficient. After four iterations, the change in pressure coefficient is virtuallly undetectable. Also, the source rings ahead of and behind the body have little effect on the solution, thus three sets of rings in these areas appear to be adequate, if placed within 0.3 body lengths of the nose and tail, in the x-direction. Along the body section, 10 sets of rings give a reasonable result, and increasing the number beyond this has little effect. Radially, outwards from the body, the extent to which rings are required is about two calibres, but strip lengths smaller thean this lead to a rise in the solution error. Again, about 10 radial divisions are required to give good results.

Figure 12 shows the comparison between the finite difference solution and the field source method for a field description of 3 + 10 + 3 rings by 10 rings, placed in the area -0.3, 0.0, 1.0, 1.3 with a strip height of 0.3. Clearly the accuracy is good for most of the body, with some divergence from the finite difference results at the

nose. Then, in Figs. 13 and 14, the results (pressure coefficient and Mach number) are shown for a similar calculation on a parabola of fineness ratio 5, at the same Mach number, but with a field strip height of 0.2. Yet again the agreement is encouraging.

Reducing the fineness ratio still further, to 2.5, produces a body which, for a free stream Mach number of 0.8, has transonic flow over its surface. At the point of maximum thickness, the flow is supersonic and so it continues to accelerate as the body narrows down, before being compressed through a shock wave. The pressure distribution, therefore, is not symmetrical about the middle of the body length.

With no damping on the equations, that is a zero value of k_v in 4.3.1, the pressure distribution for 3 + 10 + 3 by 10 rings in the area -0.3, 0.0, 1.0, 1.3, having a strip height of 0.2, is shown in Fig. 15. Over the nose and tail, the results are good, and converged, but where there is supersonic flow the distribution is poorer. In particular, the results are not converging, and no shock is present. By putting in some damping, say $0<k<0.5$, the results do converge but the distribution is still not a

To obtain a non-symmetrical pressure distribution, the number of rings down the body length has to be increased to around 30 or more, and now further axial segments are required in the source distribution in order that it has sufficient flexibility to match the surface boundary conditions. This obviously increases the amount of computation dramatically, and also the rate of convergence throughout the field is reduced. Within the limits of our VAX system, no shock waves have been found, presumably because the variation of potential in the field has not sufficient freedom.

4.4.2 Ellipsoid with a Fineness Ratio of Five.

Having now looked at the results for a pointed shape, let us consider the results for an ellipsoid with a fineness ratio of five. In all the cases, here, the field distribution was 3 + 15 + 3 by 10 rings, in the area -0.3, 0.0, 1.0, 1.3 with a strip height of 0.3. At each of the three Mach numbers 0.4, 0.6 and 0.8 the flow is wholly subsonic, and the field source method predicts the minimum value of the pressure coefficient to within 1% of the finite difference solution at the first two conditions, and to within 3.5% at the latter. Figure 16 shows the comparison in pressure coefficient distribution between the field source method and the finite difference solution. Quite clearly the differences between the two solutions are very small, with the field source method giving an accurate prediction of the stagnation pressure, the rapid acceleration over the nose region, and the flattening out of the pressure distribution.

4.4.3 A Sphere.

Unfortunately the results for a sphere are not very encouraging. Within the limitations imposed by the VAX system, both in terms of storage and run time limits, an insufficient number of field patches can be used. At a Mach number of 0.4, all of the results that we have obtained have had a minimum value of pressure coefficient below that of the finite difference soltuion. The trend appears to be that the results converge at a value close to the finite difference value. However only by adding more patches will the truth be known.

5. CONCLUDING REMARKS

From the preceding study of the various methods of allowing for compressibility effects, the Gothert-type linearisation is the simplest to apply, in that only body and velocity scalings are carried out, in association with a standard incompressible flow solution technique. For small velocity perturbations, or low free stream Mach numbers, and wholly subsonic flow, the results are quite good. However, when the flow over a blunt body at a high subsonic Mach number is computed, both the stagnation pressure and the rapid acceleration over the nose region are poorly predicted. To improve the accuracy, the full equations must be treated, and as a Rayleigh-Janzen type of expansion is difficult to apply to general body shapes, a numerical approach must be used.

Considering the equations as being of Poisson form, with the non-linear terms defining a source distribution in the flow field, an iterative solution can be achieved. Our results show that, at subsonic speeds, the results are accurate over a range of typical weapon shapes, only four solution iterations being required in most cases. With axi-symmetric flow, the field source method is slowed down by having to integrate over each ring, and the effect is the same whether elliptic integrals or numerical techniques are used. One method of speeding up the calculation would be to abandon the concept of field sources altogether, and investigate other forms of describing the field distribution, to see if a more efficient distribution is possible. This would effectively lead to a similar approach to that of Johnson et al (Ref. 15).

Extending the method, outlined here, to three dimensions would be difficult as the source distribution in the field varies in α, r and θ and so discrete point sources would have to be used. This would probably lead to similar problems of stability to those detailed in Appendix A. Thus, if is to be described by a field source distribution, a more refined description of the potential is required.

Where the finite difference methods are difficult to apply is in satisfying accurate boundary conditions on complex configurations, as well as gridding up the field volume. By comparison, the incompressible techniques already match the boundary conditions very accurately, and the complex geometries are easily dealt with. Adding sources in the field to these methods does not alter any of this. Further, only limited volumes of the flow require the sources to be placed within them whereas the present finite difference methods have grids throughout the flow field. For fully 3-dimensional configurations, the restriction on the finite difference solutions in satisfying the boundary conditions may perhaps be overcome by combining the singularity methods with finite difference methods, where the singularities match the boundary conditions. Thereby, only a restricted amount of differencing is required in areas of interest.

REFERENCES

1. CHRISTOPHER, P.A.T.
SHAW, C.T.
Generation of axi-symmetric body shapes in subsonic flow by means of polynomial distributions of sources and doublets along the axis of symmetry.
Cranfield Institute of Technology, College of Aeronautics Memo 8110, October 1981

2. CHRISTOPHER, P.A.T.
SHAW, C.T.
The use of polynomial source and doublet distributions in the lifting characteristics of axi-symmetric bodies - boundary layer influence.
Cranfield Institute of Technology, College of Aeronautics Memo 8211, May, 1982

3. CHRISTOPHER, P.A.T.
SHAW, C.T.
The use of multi-poles for calculating the aerodynamic interference between bodies of revolution in subsonic flow.
Cranfield Institute of Technology, College of Aeronautics Memo 8301, February 1983.

4. CHRISTOPHER, P.A.T.
SHAW, C.T.
The use of multi-poles for calculating the aerodynamic characteristics of bodies with elliptic cross-sections.
Cranfield Institute of Technology, College of Aeronautics Report 8324, October 1983.

5. LIEPMANN, H.W.
ROSHKO, A.
Elements of Gasdynamics
John Wiley, 1957.

6. KUTLER, P.
A perspective of theoretical and applied computational fluid dynamics.
AIAA Annual Conference, Reno, January 1983.

7. HESS, J.L.
SMITH, A.M.O.
Calculation of potential flow about arbitrary bodies.
Progress in Aeronautical Sciences, Volume 8, Pergamon, 1967.

8. ALBONE, C.M.
FORTRAN programmes for axi-symmetric potential flow about close and semi-infinite bodies.
ARC CP 1216, 1972.

9. LANDWEBER, L. The axially symmetric potential flow past elongated odies of revolution. David W. Taylor Model Basin Report 761, 1951.

10. BAKER, T.J. A computer programme to compute transonic flow over an axi-symmetric solid body. ARA Memo 197.

11. VAN DYKE, M. Perturbation Method in Fluid Mechanics. Annotated Edition, The Parabolic Press, 1975.

12. KAPLAN, C. The flow of a compressible fluid past a sphere. NACA TN 762, May 1940.

13. KELLOGG, O.D. Foundations of Potential Theory. Dover, 1953.

14. SLOOFF, J.W. Some new developments in exact integral equation formulations for sub- or transonic potential flow. NLR MP 82024 U, 1982.

15. JOHNSON, F.T.
JAMES, R.M.
BUSSOLETTI, J.E.
WOO, A.C.
A transonic rectangular grid embedded panel method.
AIAA Journal, 82-0953, 1982

16. REYHNER, T.A.
Transonic potential flow about three-dimensional inlets, ducts and bodies.
AIAA Journal, 19, 9, pp 1112-1121, September 1981.

17. GRADSTEIN, I.S.
RYSHIK, I.M.
Tables of Series, Products and Integrals.
Academic Press, 1965.

18. NUMERICAL ALGORITHMS GROUP
NAG FORTRAN Library Manual, Mark 9, Volume 5, 1982.

19. KUCHEMANN, D.
The Aerodynamic Design of Aircraft.
Pergamon, 1978.

APPENDIX A. STABILITY OF THE FIELD DISTRIBUTION CALCULATIONS

Although the use of discrete ring sources to describe the divergence of the field is conceptually simple, problems arise when setting up the field equations 4.1.5. If a source ring and field point are coincident (angle K=270 degrees in Fig. 10, for Θ =0), the integrals 4.2.6 are singular, and the solution degenerates. To overcome this, the field points can be placed in between the ring positions and a solution found. Yet again the solution degenerates, giving large values for each ring strength which oscillate in sign. Quite clearly the discrete ring description is a far-field approximation, and so the ring points and field points must be as far away from each other as possible. One way of achieving this is to integrate only the source function in the field from k=0 to 180 degrees inclusive, see Fig. 10. This however would appear a non-physical solution, and so must be justified.

Equation 4.1.5 is a non-linear partial differential equation in x and r, which has to be solved by an iteration procedure. The potential function, ϕ, is split into two main components (4.1.9); a distribution on the axis ϕ_A and a distribution in the field ϕ_F . By differentiating these functions, neither of which are solutions of 4.1.5 by themselves, the field equation 4.1.5 and the boundary condition 4.1.7 can be written as a set of linear equations which must be solved iteratively. Now, the function of x and r provided that it can be differentiated to give the derivatives required in 4.1.5 and 4.1.7. Using the half-ring approach gives a rapidly convergent solution where both 4.1.5 and 4.1.7 are satisfied in the field and on the surface respectively. All the results shown in this report for the field source method are derived using this approach.

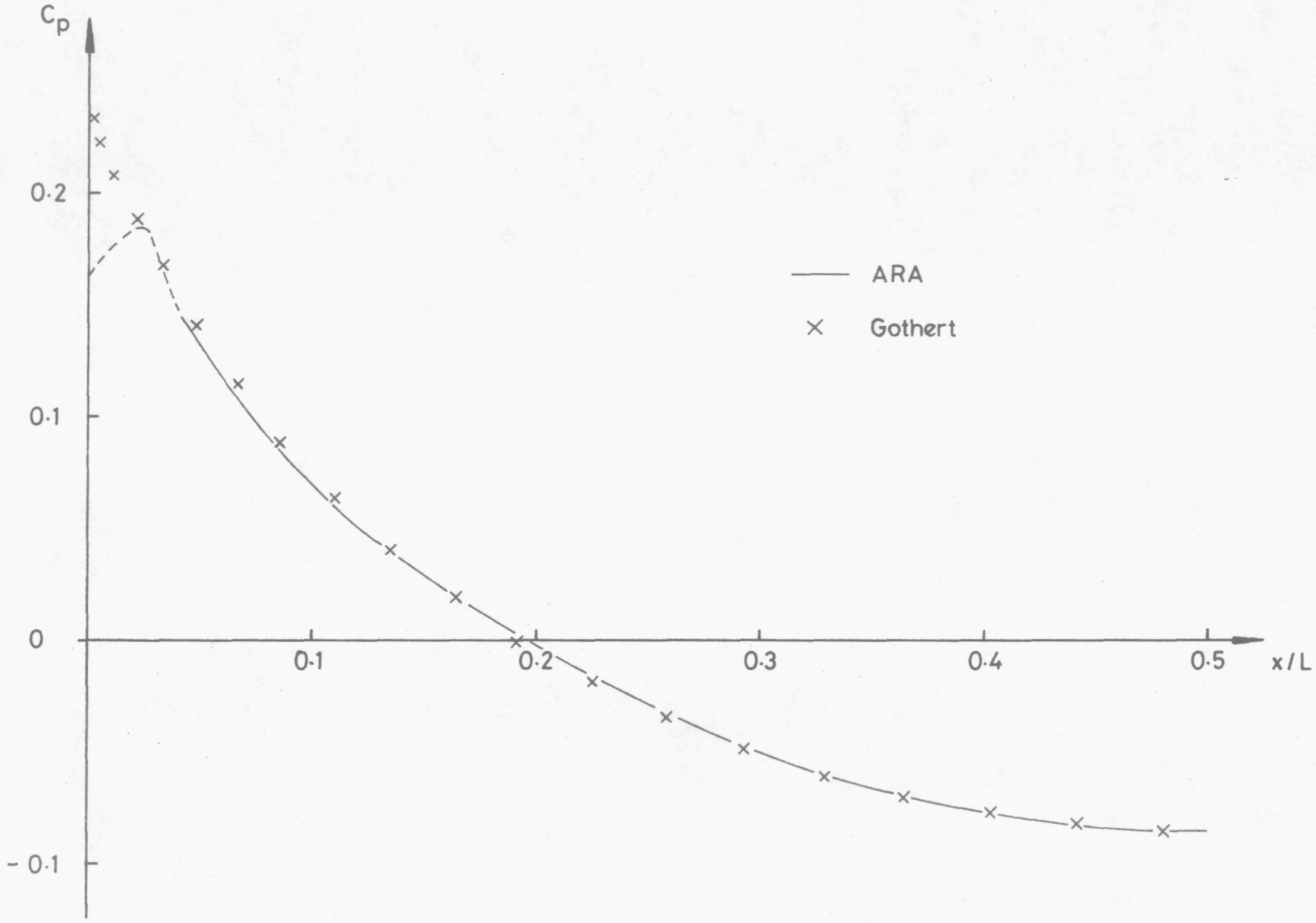

Fig.1. Pressure Distribution on Paraboloid of Revolution, $M_\infty = 0.8$.

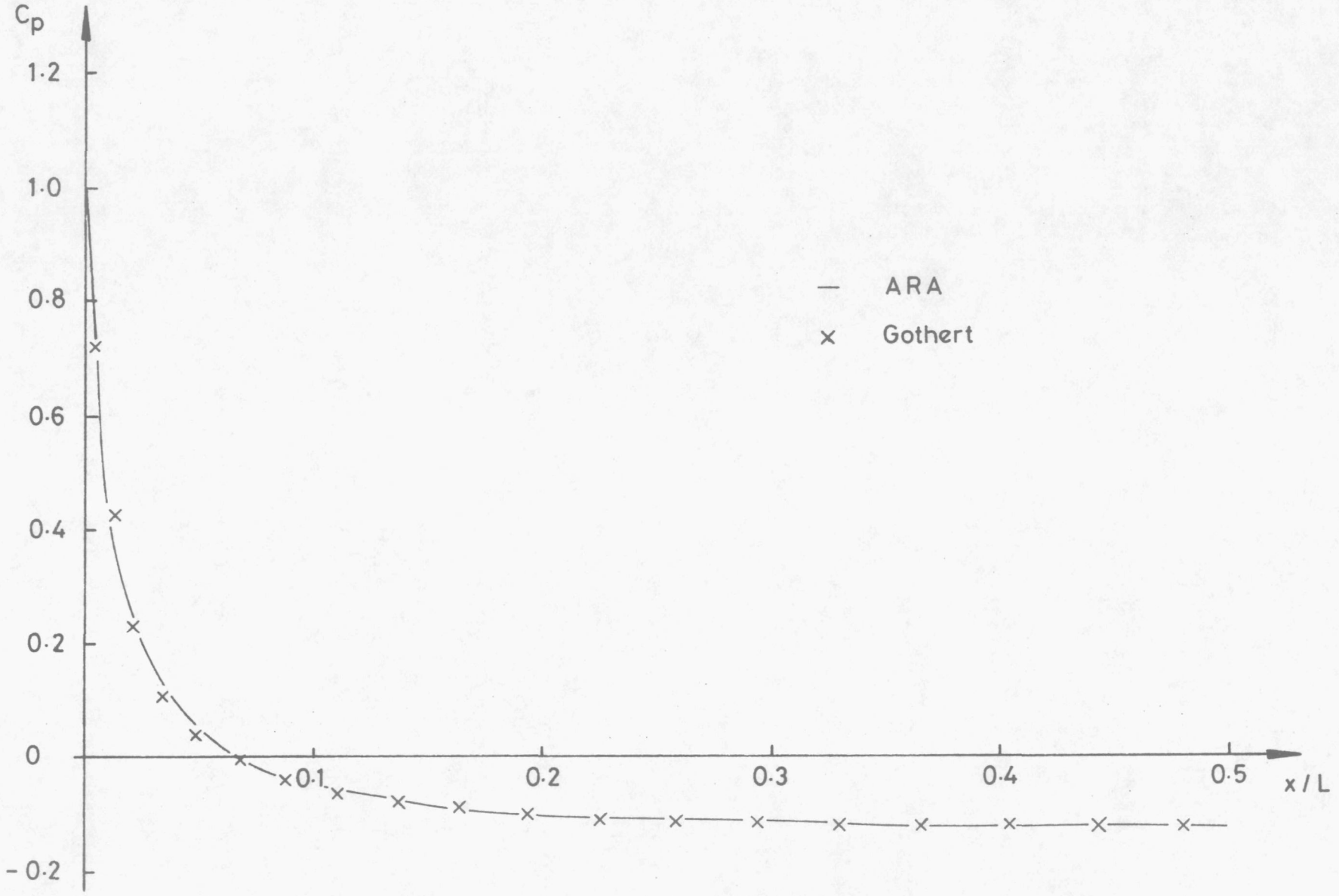

Fig. 2. Pressure Distribution on Ellipsoid, $M_\infty = 0.4$.

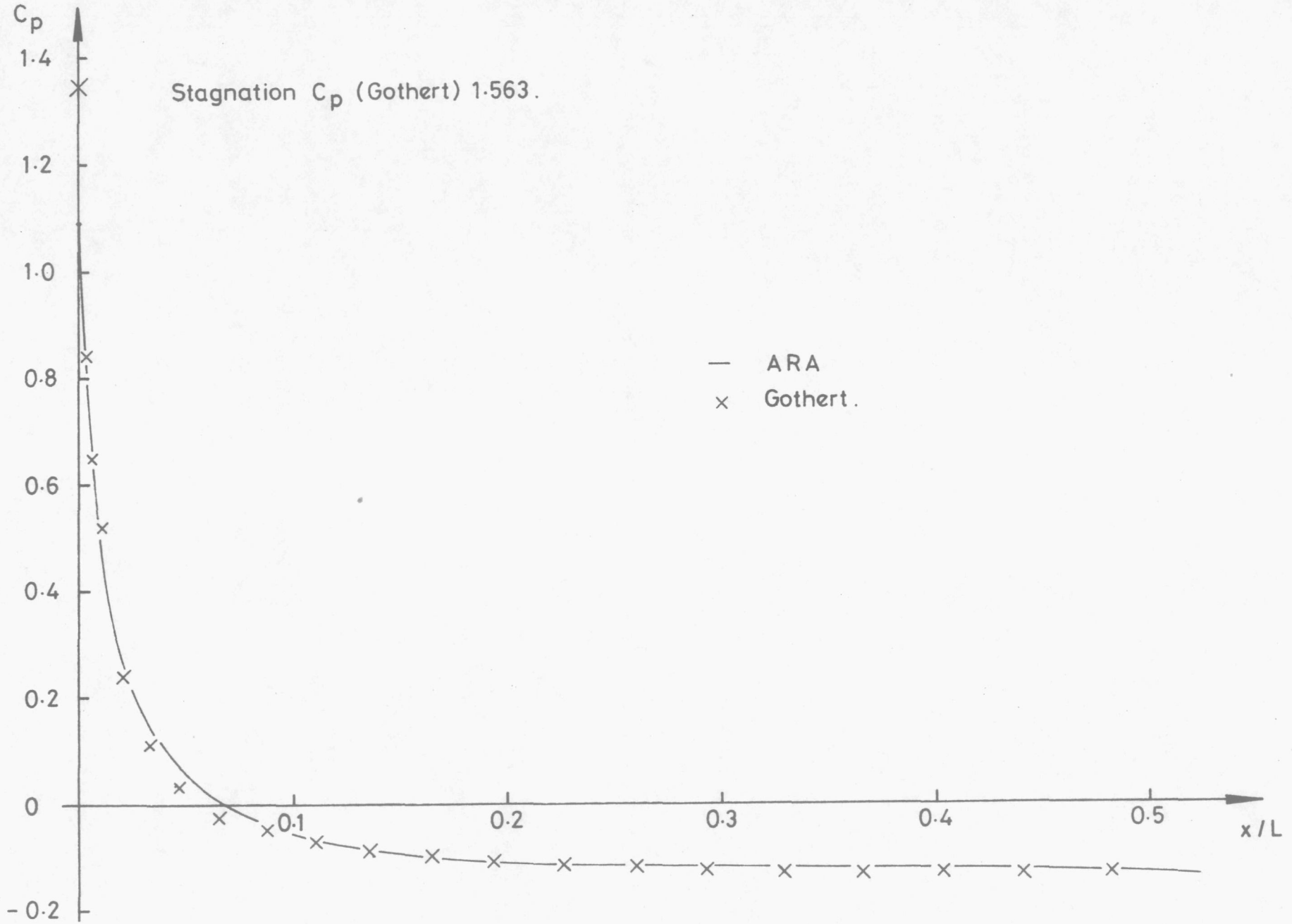

Fig.3. Pressure Distribution on Ellipsoid, $M_\infty = 0{\cdot}6$.

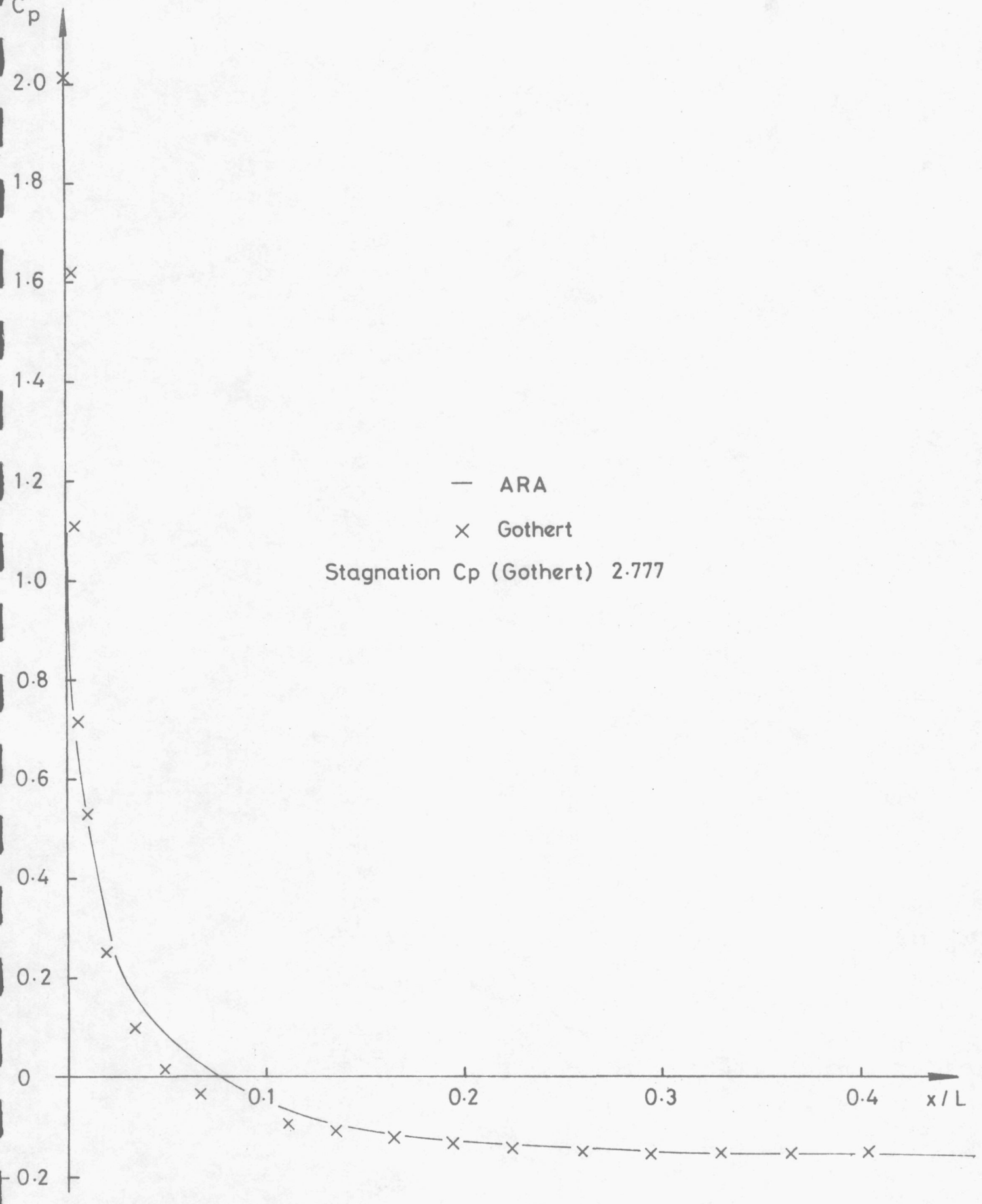

Fig. 4. Pressure Distribution on Ellipsoid, $M_\infty = 0.8$.

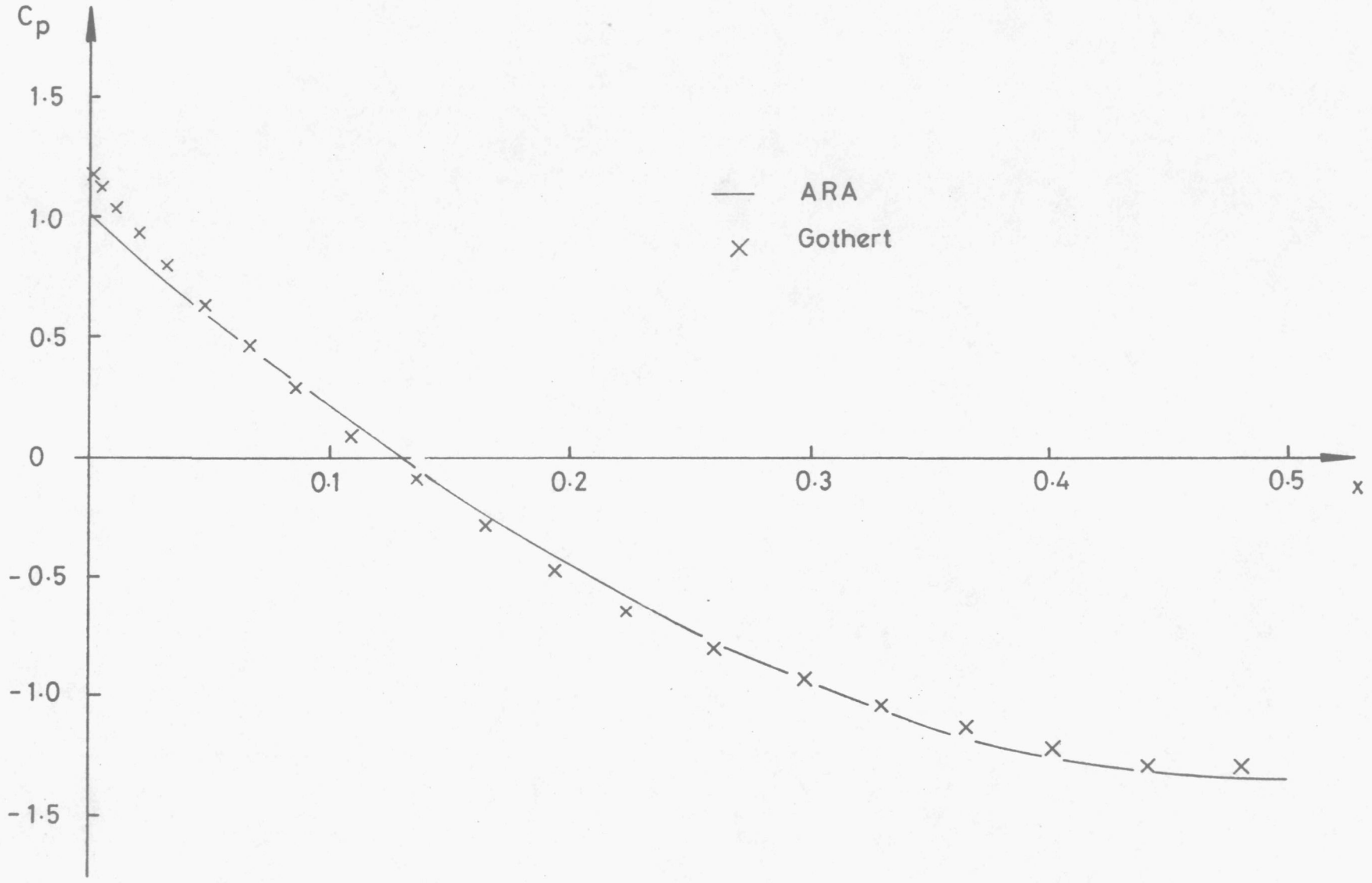

Fig. 5. Pressure Distribution on Sphere, $M_\infty = 0{\cdot}4$.

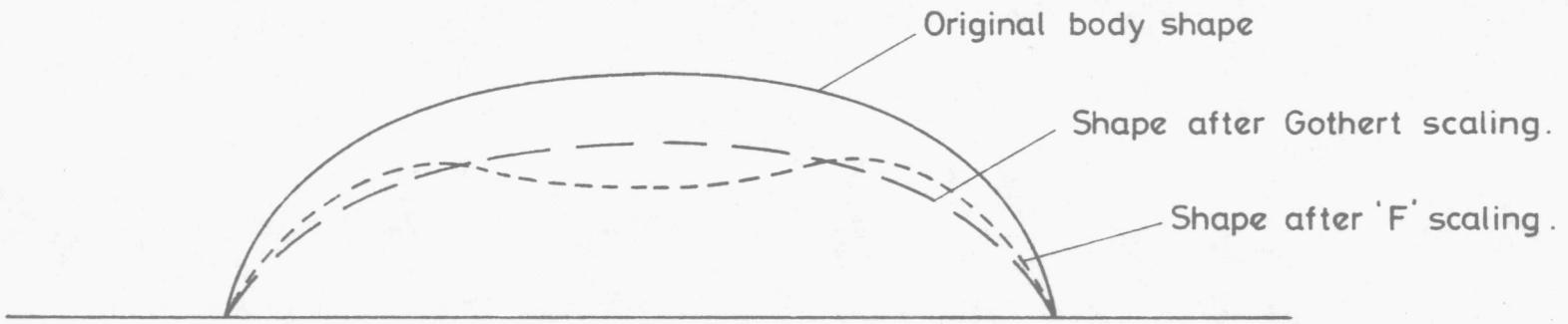

Fig.6. The Effect of Scaling on Body Shape.

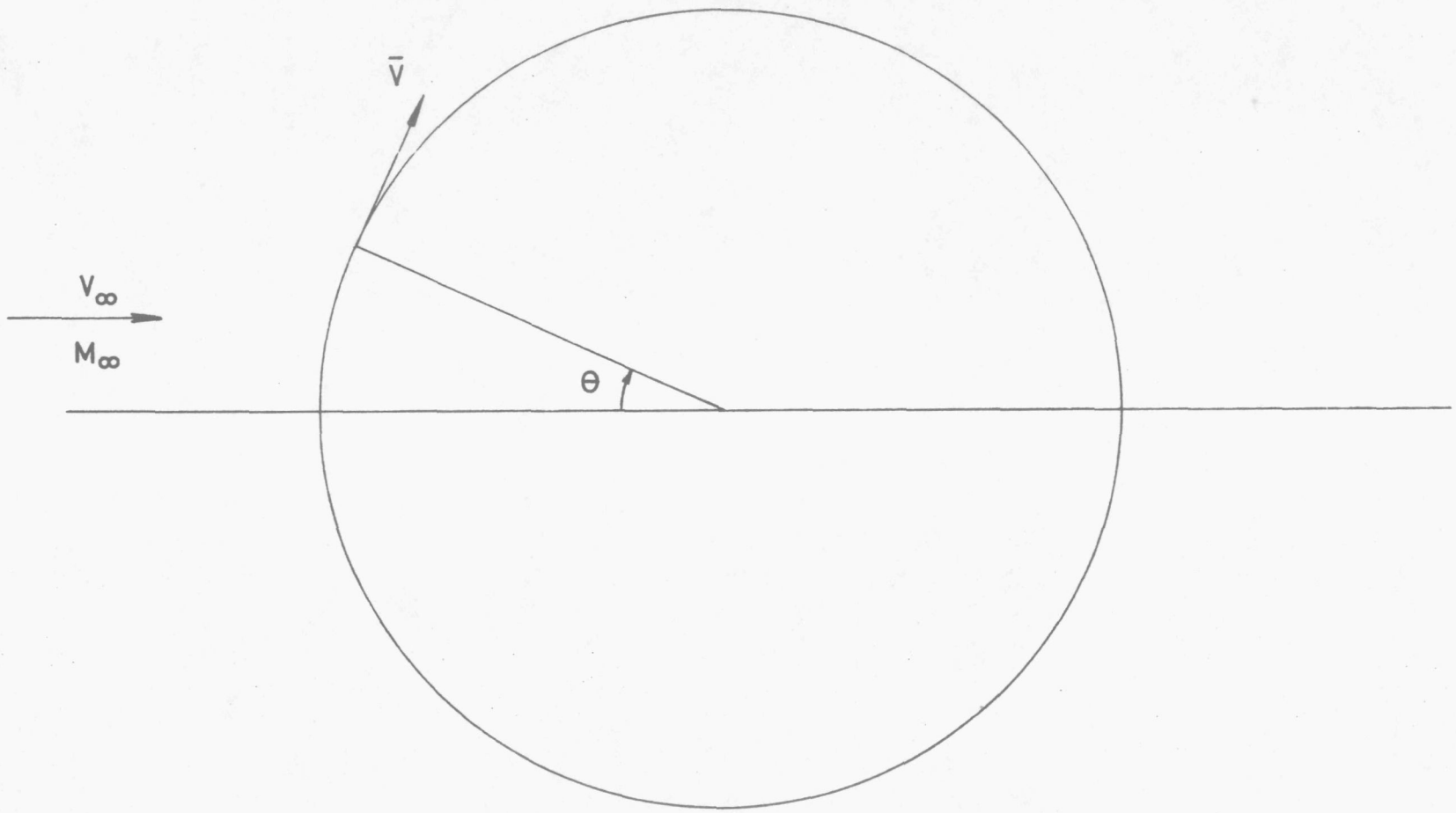

Fig.7. A Sphere in Compressible Flow.

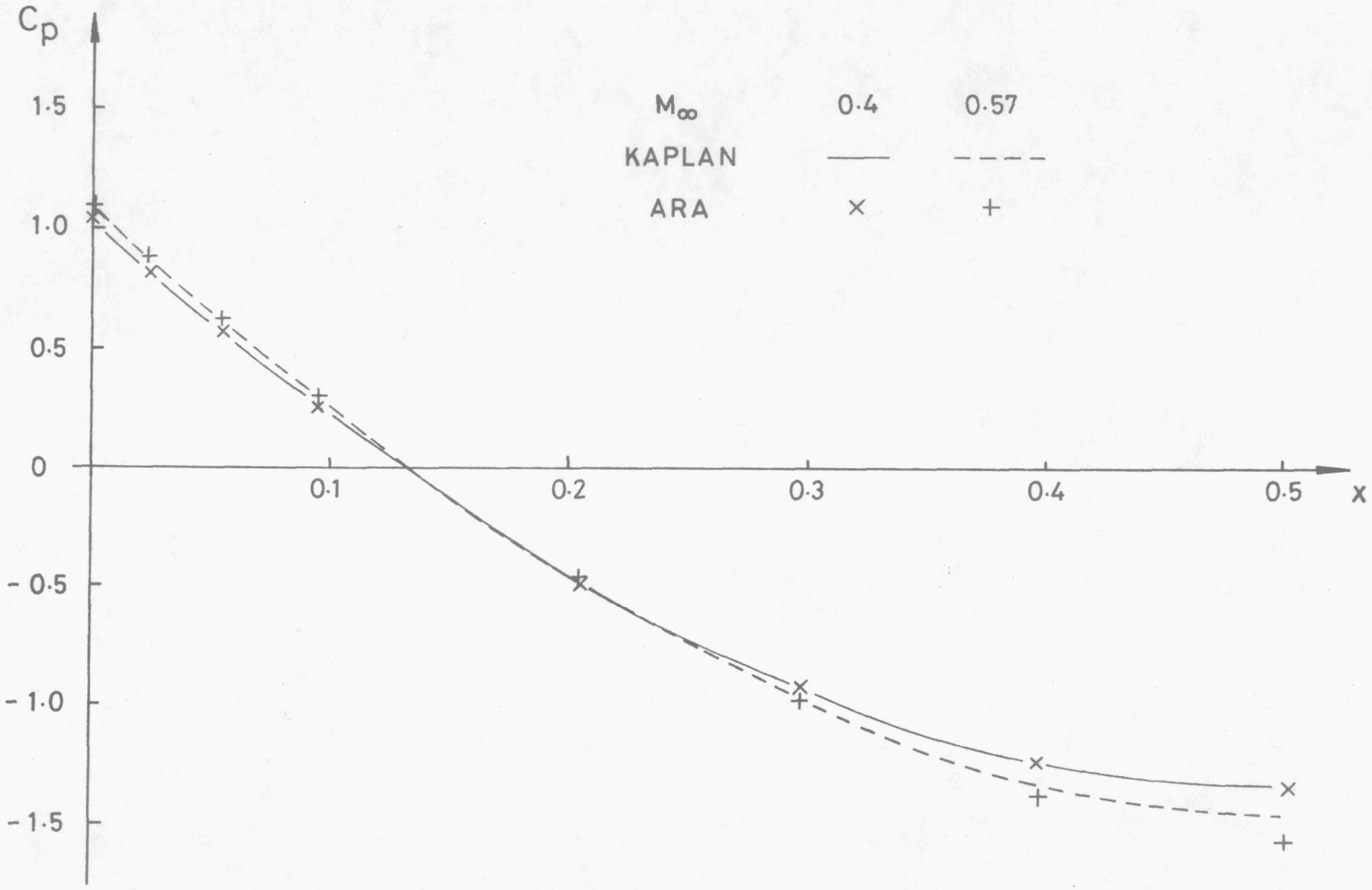

Fig. 8. Comparison of Kaplan's Results with ARA Results for Sphere.

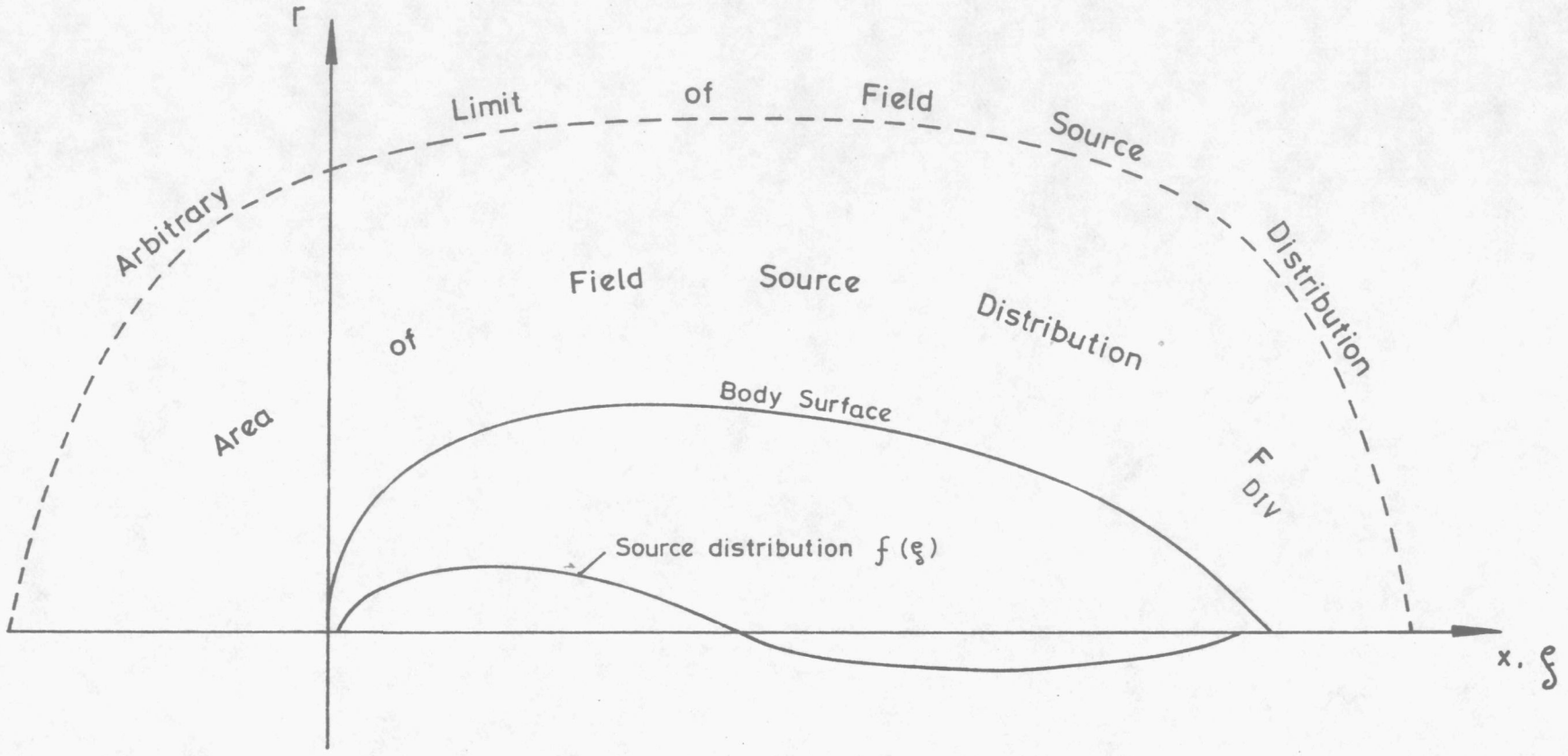

Fig.9. The Field Source Problem.

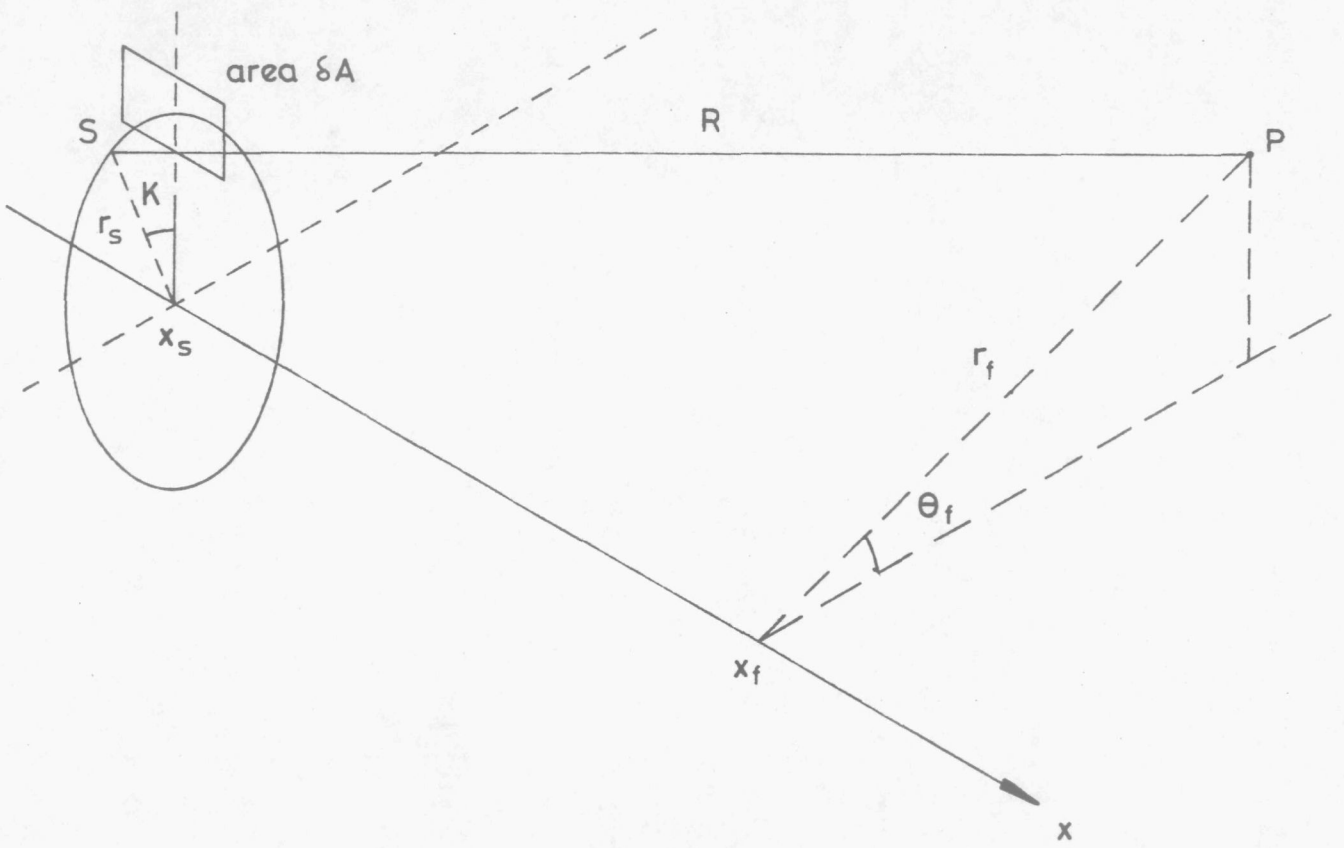

Fig. 10. The Source Ring.

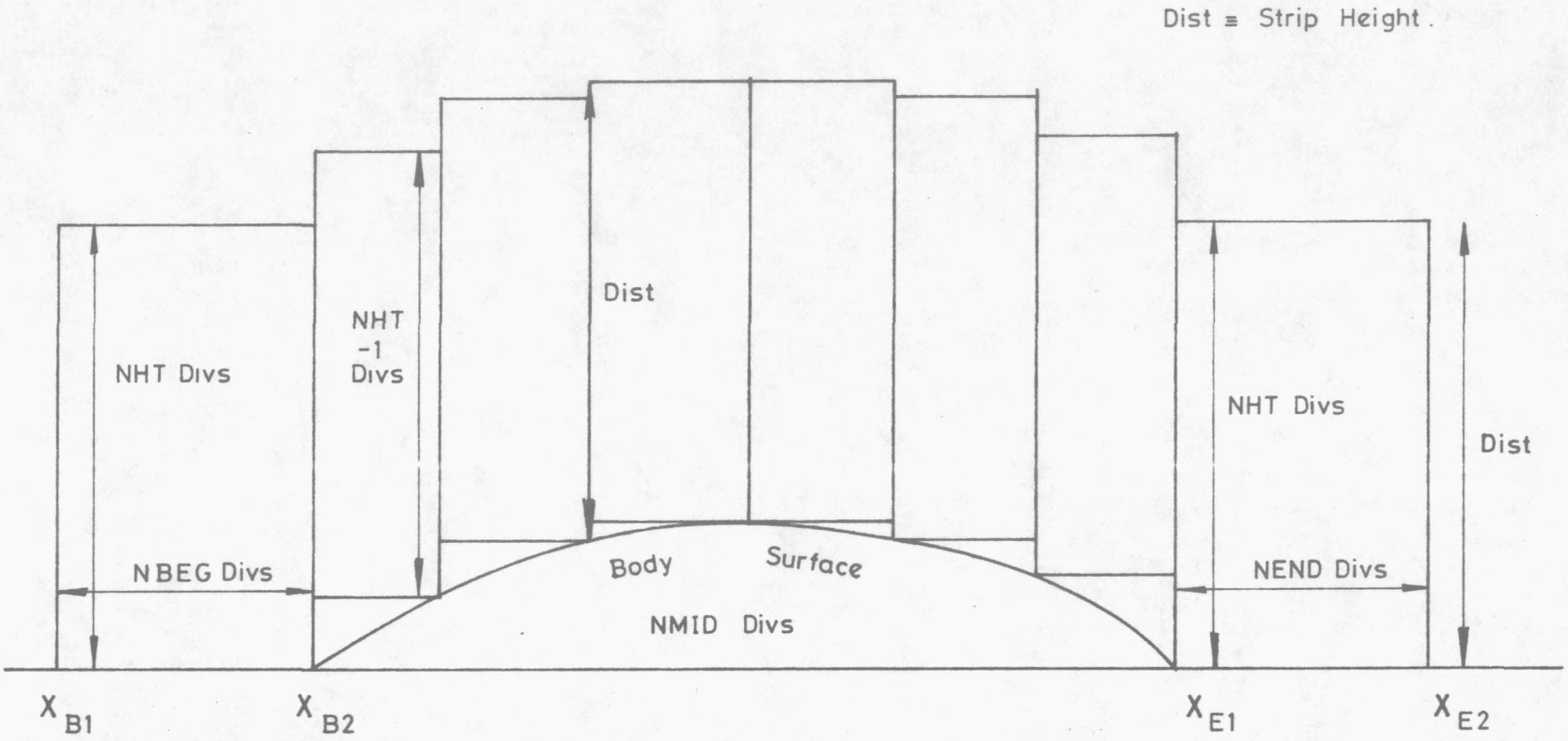

Fig.11. The Field Source Distribution Parameters.

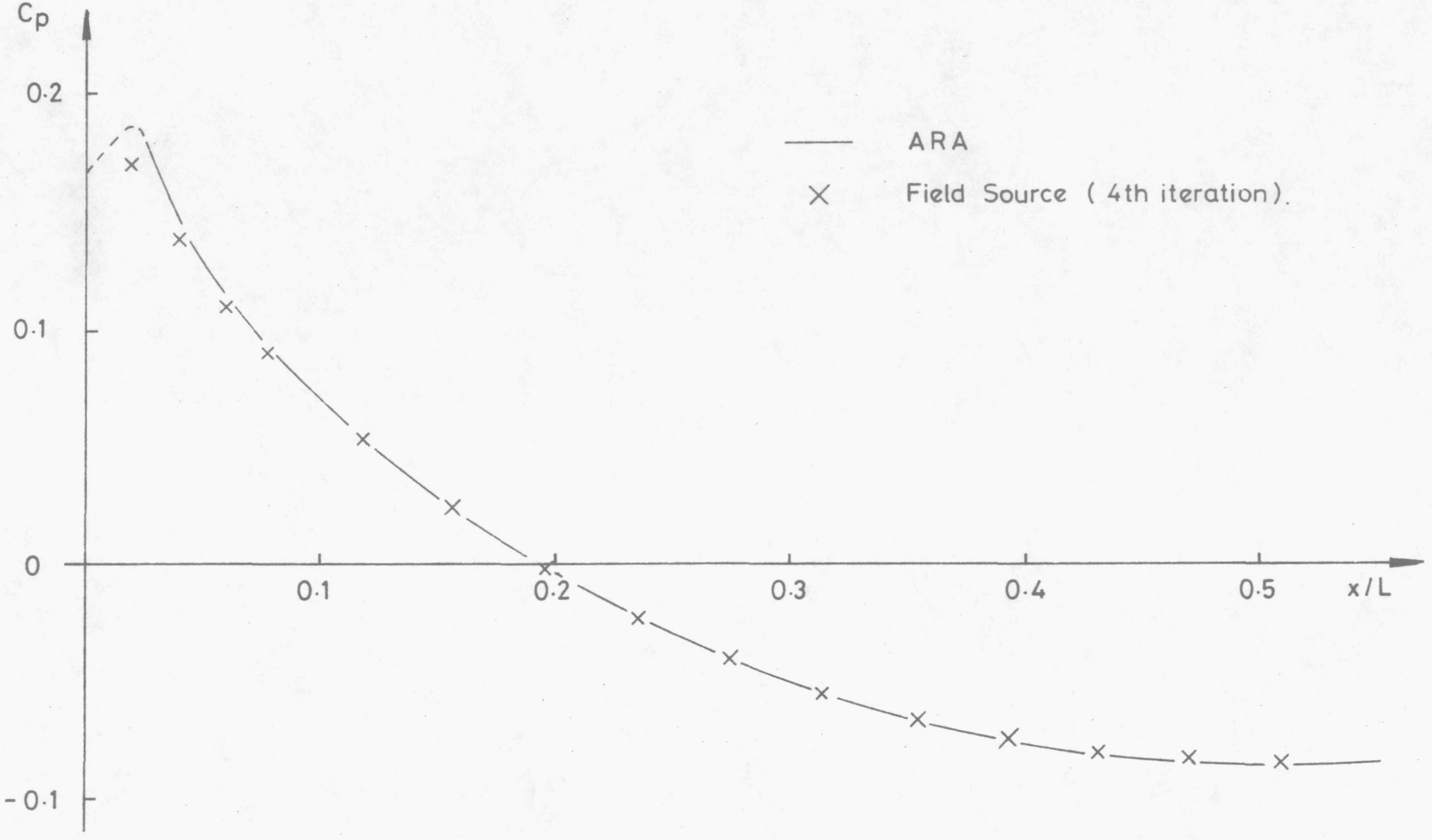

Fig. 12. Pressure Distribution on Paraboloid, Fineness Ratio 10, $M_\infty = 0.8$.

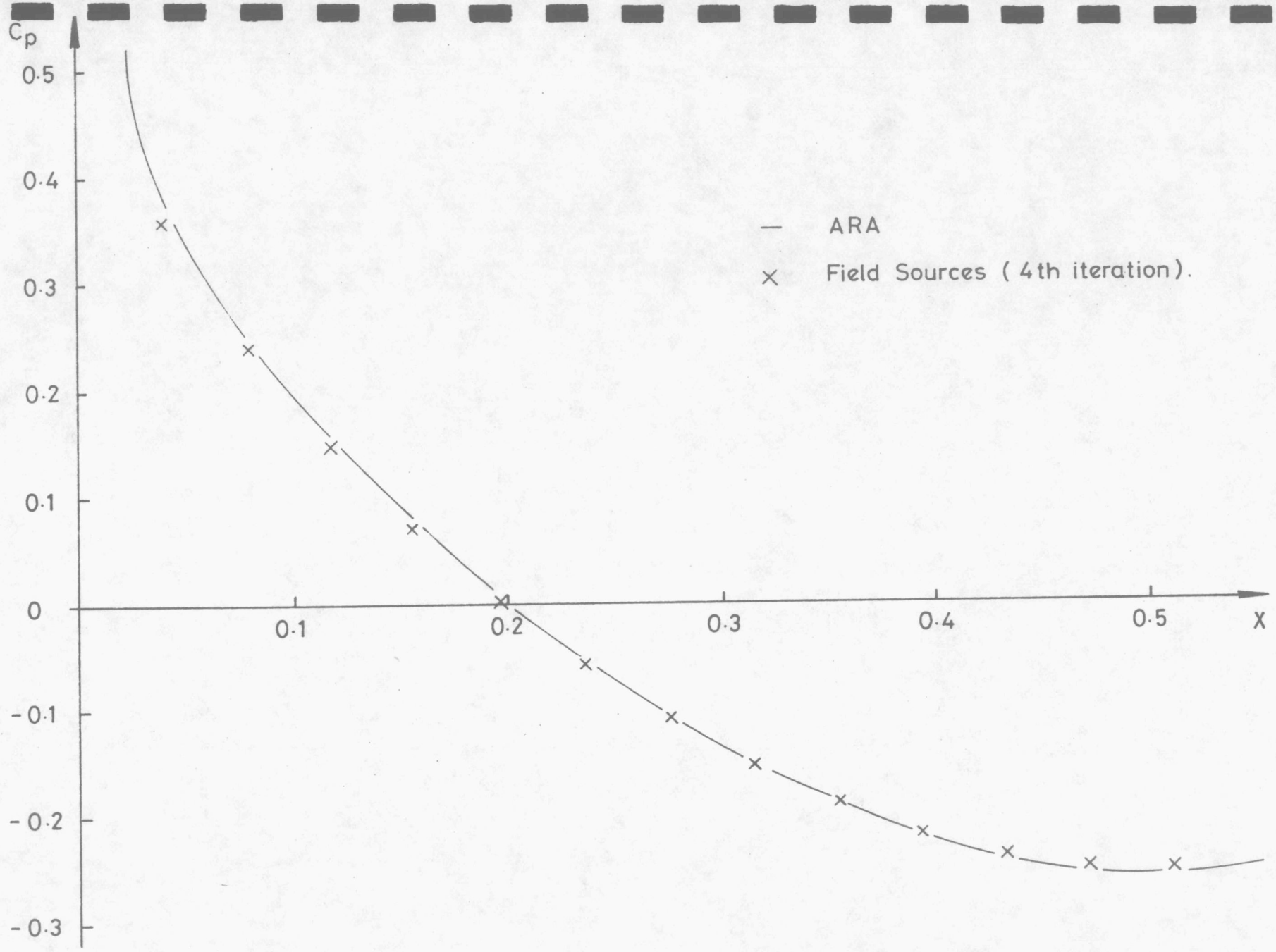

Fig. 13. Pressure Distribution on Paraboloid, Fineness Ratio 5, $M_\infty = 0.8$.

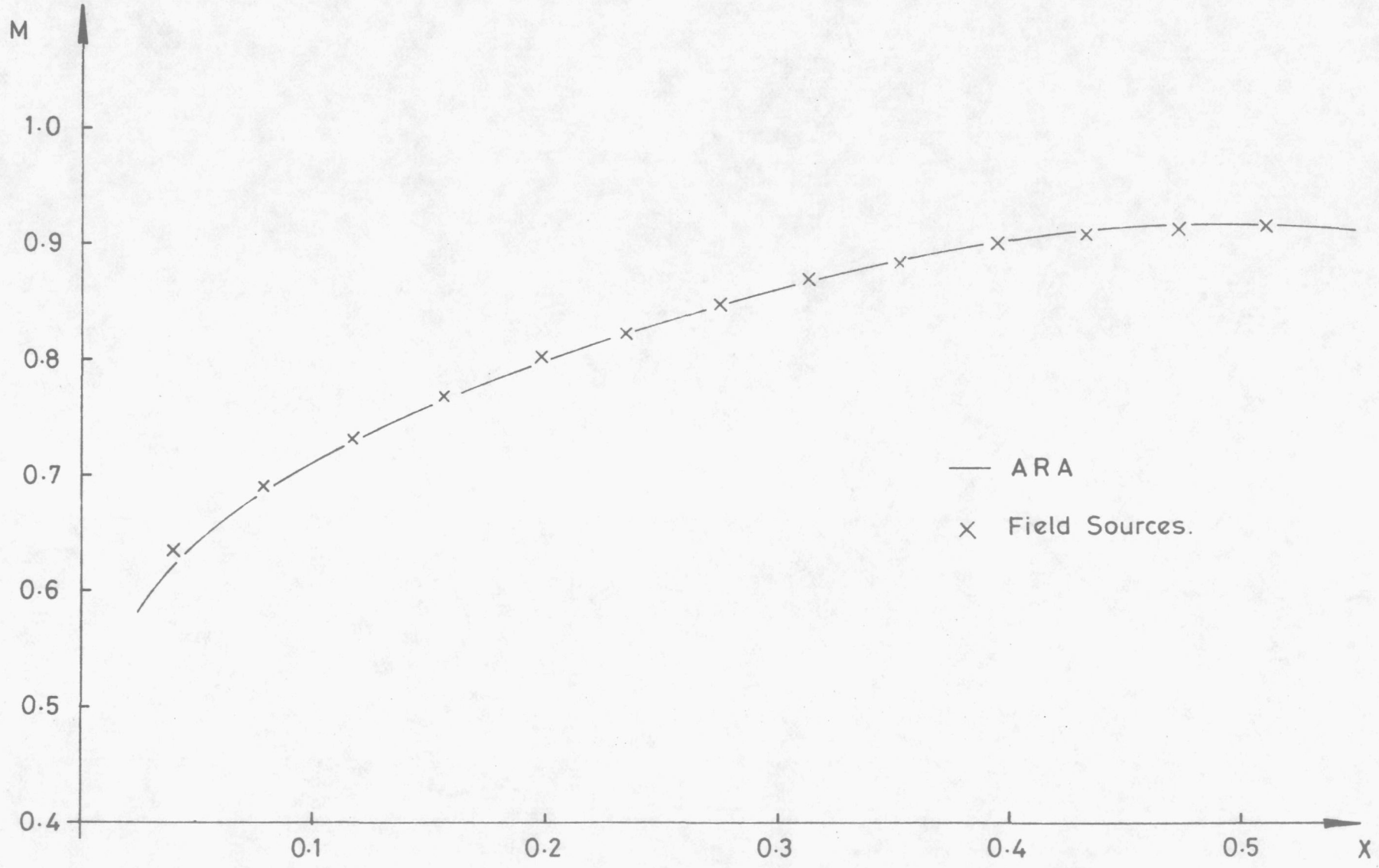

Fig.14. Mach Number Distribution on Paraboloid of Fig 13.

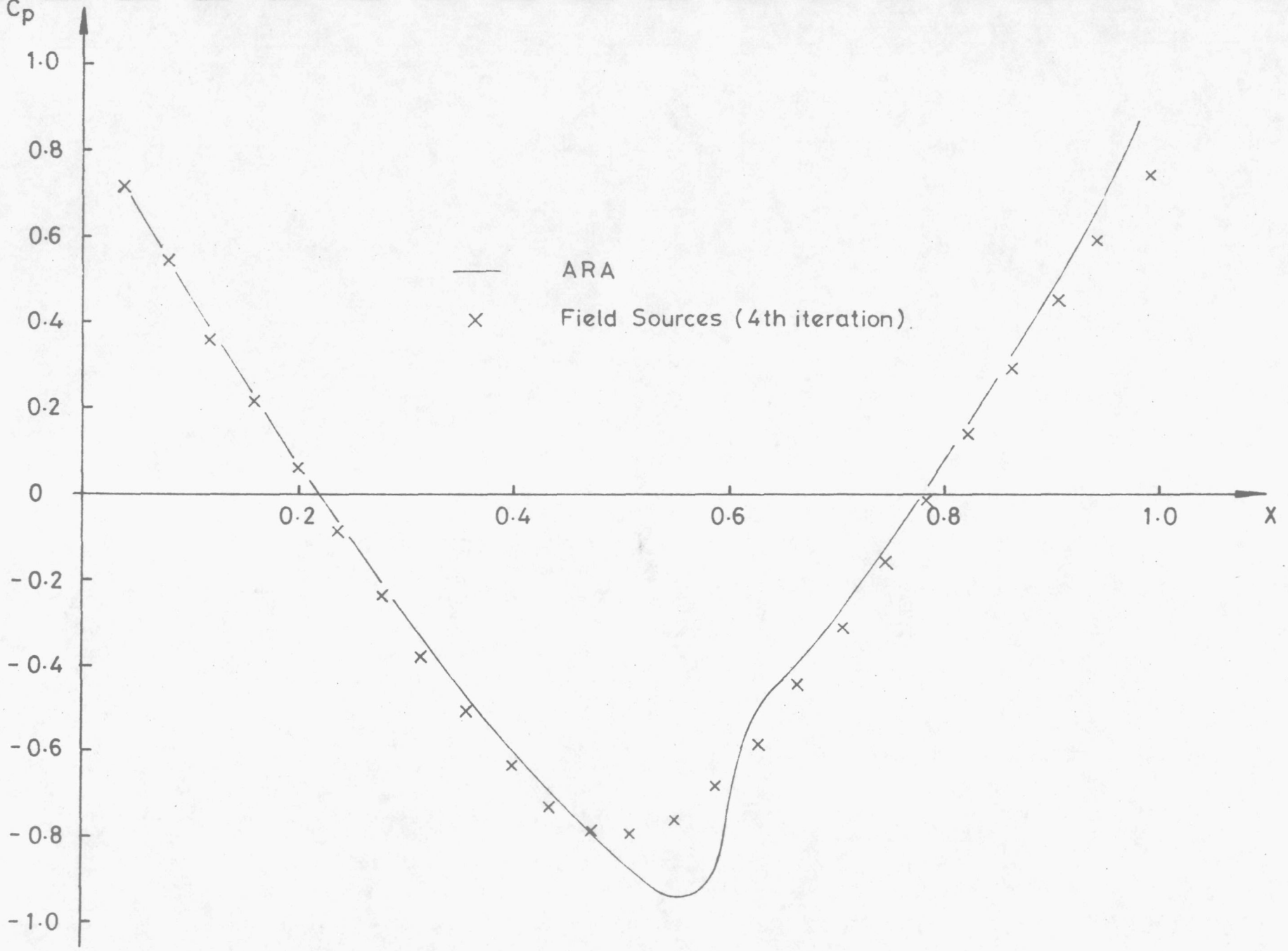

Fig.15. Pressure Distribution on Paraboloid, Fineness Ratio 2·5, $M_\infty = 0·8$.

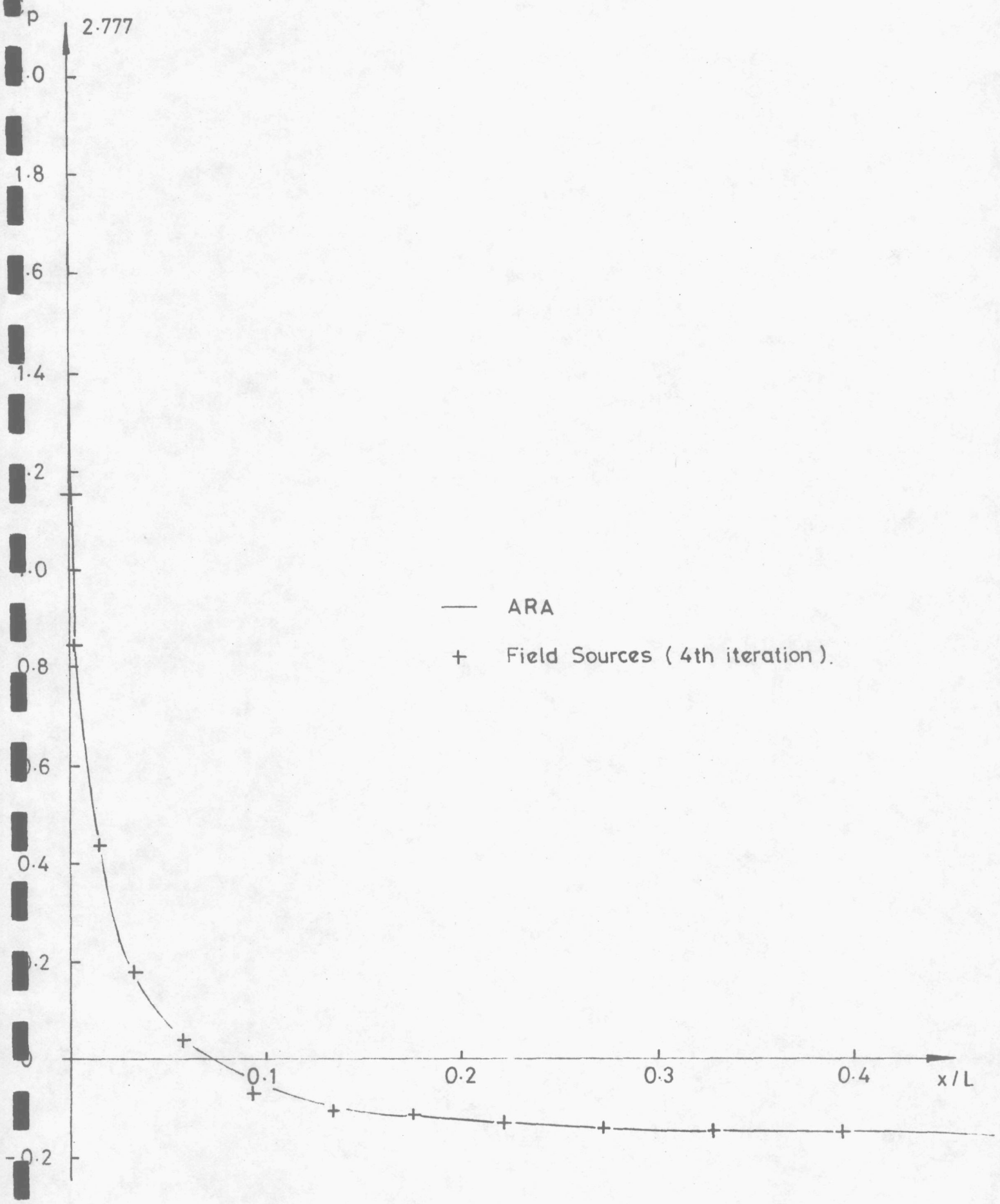

Fig. 16. Pressure Distribution on Ellipsoid, $M_\infty = 0.8$.